



## OPEN ACCESS

## EDITED BY

Gustavo A. Patow,  
University of Girona, Spain

## REVIEWED BY

Hugo Geerts,  
Certara UK Limited, United Kingdom  
Stephen Duffull,  
Certara, United States

## \*CORRESPONDENCE

Andrzej Przekwas  
✉ andrzej.przekwas@cf-d-research.com

RECEIVED 22 October 2025

REVISED 07 January 2026

ACCEPTED 16 January 2026

PUBLISHED 10 February 2026

## CITATION

Przekwas A, Norris C and Garimella HT (2026)  
Mechanistic modeling of amyloid dynamics  
relating to Alzheimer's disease progression.  
*Front. Aging Neurosci.* 18:1730480.  
doi: 10.3389/fnagi.2026.1730480

## COPYRIGHT

© 2026 Przekwas, Norris and Garimella. This is an open-access article distributed under the terms of the [Creative Commons Attribution License \(CC BY\)](https://creativecommons.org/licenses/by/4.0/). The use, distribution or reproduction in other forums is permitted, provided the original author(s) and the copyright owner(s) are credited and that the original publication in this journal is cited, in accordance with accepted academic practice. No use, distribution or reproduction is permitted which does not comply with these terms.

# Mechanistic modeling of amyloid dynamics relating to Alzheimer's disease progression

Andrzej Przekwas\*, Carly Norris and Harsha T. Garimella

Biomedical, Energy, and Materials Division, CFD Research Corporation, Huntsville, AL, United States

The use of mechanistic models to support personalized medicine and precision diagnostics offers transformative potential for neurology. In this study, we developed a mechanistic model of Alzheimer's Disease progression (mAD) that integrates amyloid precursor protein (APP) processing, A $\beta$  peptide generation, A $\beta$  aggregation pathway modeling, A $\beta$  transport, and whole-body biomarker kinetics (BxK) of A $\beta_{40}$  and A $\beta_{42}$  peptides, including enzymatic and microglial clearance mechanisms. The purpose of this work was to formulate an integrated, multiscale quantitative systems pharmacology (QSP) mechanistic model of Alzheimer's progression to advance neuroscience QSP frameworks. The model described in this work provides a basis for personalized precision neurology with the potential to facilitate pre-symptomatic AD diagnosis, thereby establishing early prevention strategies, and accelerating identification of optimal therapeutic interventions.

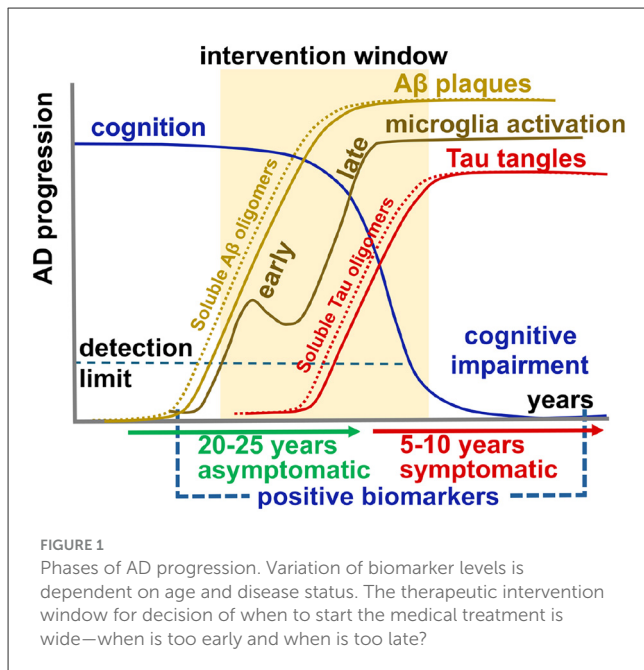
## KEYWORDS

Alzheimer's disease, amyloid pathology, apolipoprotein E, biomarker kinetics, quantitative systems pharmacology

## 1 Introduction

Alzheimer's disease (AD) is the most common neurodegenerative disorder, affecting up to 20% of individuals over 80 years old. It is a progressive disease characterized by a prolonged preclinical (asymptomatic) phase, an early prodromal stage (mild cognitive impairment, MCI), and a more rapidly advancing dementia stage involving significant cognitive and functional decline (Vermunt et al., 2019). Recent global estimates indicate that up to 100 million individuals currently present with symptomatic forms of AD, including MCI (Nichols et al., 2022; Gustavsson et al., 2023). Epidemiological studies show that the number of dementia cases is rising as populations age (Prince et al., 2016), underscoring the urgent need for early diagnostics and treatments, even among asymptomatic populations.

The clinical manifestation of AD is heterogeneous in both severity and the underlying pathology, which includes the distribution and composition of extracellular A $\beta$  deposition, spread of intracellular tau protein tangles, chronic neuroinflammation, and deterioration of cognitive functions (Knopman et al., 2021). Life-long AD progression phases have been previously defined based on trajectories of detectable biomarkers, as indicated in Figure 1 (Jack et al., 2013b; McDade et al., 2020; Oumata et al., 2022; Leng and Edison, 2021; Fišar, 2022). These AD progression events occur within a wide therapeutic intervention window for decision when to initiate medical treatment. Heterogeneity in AD may be related to various risk factors: genetics, demographics (age, sex, and educational level), comorbidities (hypertension, diabetes), and other modifiable factors (addictions, obesity, smoking, and



depression) (Bellenguez et al., 2022; Omura, 2022; Seemiller et al., 2024; Allwright et al., 2023). Early detection of biomarkers and identification of at-risk individuals may help establishing prevention measures and more effective treatments to delay the onset and slow down disease progression (Niotis et al., 2024).

The complex nature of neurodegenerative diseases makes it difficult to develop accurate diagnostics and effective therapies. Over the last decade, a growing body of data from *in vitro* neurobiology, clinical neuroimaging, and biomarker kinetics data has supported the development of mechanistic mathematical models of AD pathophysiology and pharmacology (Karelina et al., 2021; Ferl et al., 2020; Madrasi et al., 2021; Lin et al., 2022; Bloomingdale et al., 2021). Traditional neuropharmacology models have typically focused on a single domain, such as A $\beta$  biology, pharmacokinetics (PK), target binding of small molecules, or neuroimaging, limiting their scope and influence. In contrast, quantitative systems pharmacology (QSP) has emerged as a multiscale, multidisciplinary computational framework integrating systems biology, population PK, pharmacodynamics (PD), effects of risk factors including genetics, biomarker kinetics (BxK), adverse reactions to medication, neuroimaging, and disease progression (Lin et al., 2022; Clausznitzer et al., 2018; Geerts et al., 2023b, 2020, 2024a; Ramakrishnan et al., 2023). Several subset QSP models have been developed to investigate key mechanisms known to contribute to AD, such as A $\beta$  generation, aggregation and biodistribution in body fluids, activation and engagement of microglia, the PK of biologics-based immunotherapies, and the PD of drug interaction with A $\beta$  structures (Lin et al., 2022; Bloomingdale et al., 2021; Clausznitzer et al., 2018; Geerts et al., 2023b, 2020, 2024a; Ramakrishnan et al., 2023; Bloomingdale et al., 2022; Marković et al., 2024). These computational QSP models have the potential to enhance our mechanistic understanding of AD, accelerate the development of safe and efficacious therapeutics, enable earlier and more accurate diagnosis,

and support personalized treatment strategies (Hampel et al., 2020).

The purpose of this work was to formulate an integrated, mechanistic model of AD progression by combining multiple subset QSP models to advance the broader field of neuroscience QSP. Continued integration of complex models into a single framework has the potential to support a forthcoming revolution in personalized precision neurology (Hampel et al., 2020, 2018), enabling pre-symptomatic AD diagnosis, and development of early preventive and optimal therapeutic interventions.

## 2 Materials and methods

### 2.1 Overview

The mechanistic model of AD (mAD) progression developed in this study integrates four main components:

- 1) Amyloid precursor protein (APP) processing in the human brain and subsequent generation of amyloid  $\beta$  (A $\beta$ ) peptides
- 2) A $\beta$  aggregation pathway modeling
- 3) A $\beta$  transport and whole-body biomarker kinetics (BxK) of A $\beta_{40}$  and A $\beta_{42}$  peptides
- 4) Enzymatic and microglial clearance of A $\beta$

For each A $\beta$  peptide, the aggregation pathway model is represented by six species: monomer (M), dimer (D), small oligomer (o), large oligomer (O), protofibril (F) and plaque (P), as indicated in Figure 2. In addition, mAD validation was conducted by comparing simulation outputs to clinical neuroimaging data, specifically evaluating A $\beta$  plaque burden using Standardized Uptake Value Ratio (SUVR) and Centiloid scales (Figure 2).

The mAD model was implemented using multiscale Computational Biology (CoBi) software version 2023.1.1, which enables physics-based numerical solutions of coupled ordinary and partial differential equations (ODEs, PDEs) for biology applications (Przekwas et al., 2006). Source coding of the pathway mechanics and parameters used in the model are available in the Supplementary material.

### 2.2 APP processing and generation of A $\beta$ peptides

A $\beta$  is a 38–43 amino acid peptide derived from APP through sequential cleavages by  $\beta$ - and  $\gamma$ -secretase enzymes in an amyloidogenic pathway. A $\beta$  generation was accounted for based on an APP processing model adapted from the work of Madrasi (Madrasi et al., 2021). However, APP is also processed in parallel by  $\alpha$ -secretase to generate soluble APP $\alpha$  in a non-amyloidogenic pathway (Figure 3) (Chow et al., 2010). When APP is cleaved by  $\alpha$ -secretase ( $\alpha$ S) followed by  $\gamma$ -secretase ( $\gamma$ S), this results in a hydrophobic p3 peptide release (also known as A $\beta_{17-40/42}$ ). Therefore, the Madrasi model was extended in this work to also include the non-amyloidogenic processing of APP. In the present mAD model, equations for all species were formulated to achieve molar balance according to the reaction mechanisms defined in

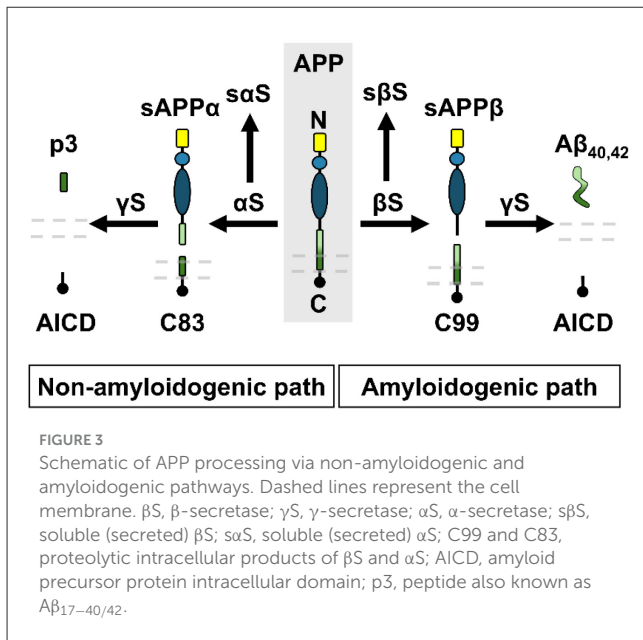
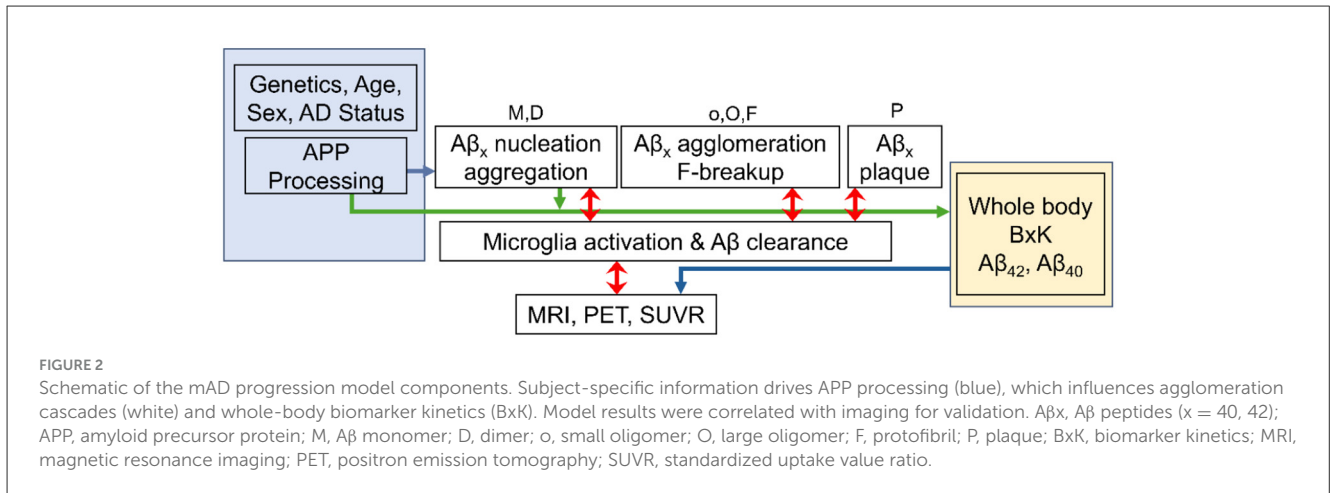


**Table 1.** These reactions were used by the CoBi ODE-Gen module to automatically generate ODEs. A two-way arrow indicates a reversible reaction, and a one-way arrow indicates an irreversible reaction at a known rate. Both pathways accounting for APP and Aβ homeostatic biogenesis are essential for synaptic function.

Various length Aβ isoforms in the human brain appear to have neuroprotective properties at low concentrations where the length of the Aβ species affects their physiological and biophysical properties. Among the various Aβ isoforms, Aβ<sub>40</sub> (~4.3 kDa) and Aβ<sub>42</sub> (~4.5 kDa) are most relevant due to their roles in AD pathology and diagnostics. These two isoforms were therefore selected for inclusion in the model.

### 2.3 Aβ aggregation pathway model

Once Aβ<sub>x</sub> monomers are generated, they become involved in a complex aggregation process forming dimers, oligomers,

protofibrils, fibrils, and ultimately plaques. The cascade involves a large number of steps including primary and secondary nucleation, oligomerization, breakup, catalytic growth, and formation of insoluble fibrils and large plaques. Assumptions for this aggregation model are based on the peptide properties.

For both Aβ<sub>40</sub> and Aβ<sub>42</sub>, the N-terminal is hydrophilic while most amino acid residues in C-terminal region (originating from the transmembrane region of APP) are more hydrophobic. Under physiological conditions, the Aβ hydrophobic C-terminal region forms a folded structure and exposes the hydrophilic N-terminal region (Song et al., 2022). In its native conformation (folded) the monomer exists as a stable structure without self-aggregation. Under certain conditions Aβ unfolds and forms a thermodynamically unstable morphology, leading to the binding of two hydrophobic C-terminals to form a more stable, aggregated dimer. This aggregation process continues, leading to higher-order aggregates.

An Aβ generation/aggregation kinetics model was recently developed by Geerts et al. (2023b), which employed a 25-step aggregation pathway for both Aβ<sub>40</sub> and Aβ<sub>42</sub>. However, the Geerts model contained a large number of parameters that had to be calibrated from limited clinical data. In this case, the large number of assumptions on aggregate size and morphology is unlikely to benefit mechanistic understanding at such a high resolution without proper calibration. In contrast, our Aβ agglomeration reduced order model (ROM) was formulated using only six Aβ species: monomer (M), dimer (D), small oligomer (o), large oligomer (O), protofibril (F) and plaque (P). A schematic of the simplified, linear, reversible aggregation pathway is shown in Figure 4A followed by the reaction kinetics for the full aggregation pathway model assumptions (Figure 4B). Model aggregation assumptions were consistent for Aβ<sub>40</sub> and Aβ<sub>42</sub>, however, since Aβ<sub>42</sub> is more hydrophobic and more prone to aggregate compared to Aβ<sub>40</sub>, it was assumed to form fibrils significantly faster. The kinetic rate constants were derived from the previously reported 25 step Aβ aggregation model (Geerts et al., 2023b). Rate constants for the monomer (M) and dimer (D) were the same as the reference model such that generation of monomers and dimerization of two monomers into a dimer were treated with full stoichiometry consistency. Rate constants for the larger species (o,O,F,P) were

TABLE 1 Reaction mechanisms of non-amylogenic and amyloidogenic processing of APP.

Generation
$0 \leftrightarrow \text{APP}$
$0 \leftrightarrow \beta\text{S}$
$0 \leftrightarrow \gamma\text{S}$
$0 \leftrightarrow \alpha\text{S}$
<b>Non-amyloidogenic pathway</b>
$\alpha\text{S} \rightarrow \text{s}\alpha\text{S}$
$\text{APP} + \alpha\text{S} \leftrightarrow \text{APP}:\alpha\text{S}$
$\text{APP}:\alpha\text{S} \rightarrow \text{C83} + \alpha\text{S} + \text{sAPP}\alpha$
$\text{C83} + \gamma\text{S} \leftrightarrow \text{C83}:\gamma\text{S}$
$\text{C83}:\gamma\text{S} \rightarrow \text{p3} + \gamma\text{S}$
$\text{s}\alpha\text{S} \rightarrow 0$
$\text{C83} \rightarrow 0$
$\text{sAPP}\alpha \rightarrow 0$
$\text{p3} \rightarrow 0$
<b>Amyloidogenic pathway</b>
$\beta\text{S} \rightarrow \text{s}\beta\text{S}$
$\text{APP} + \beta\text{S} \leftrightarrow \text{APP}:\beta\text{S}$
$\text{APP}:\beta\text{S} \rightarrow \text{C99} + \beta\text{S} + \text{sAPP}\beta$
$\text{C99} + \gamma\text{S} \leftrightarrow \text{C99}:\gamma\text{S}$
$\text{C99}:\gamma\text{S} \rightarrow \text{A}\beta_{42} + \gamma\text{S}$
$\text{C99}:\gamma\text{S} \rightarrow \text{A}\beta_{40} + \gamma\text{S}$
$\text{s}\beta\text{S} \rightarrow 0$
$\text{C99} \rightarrow 0$
$\text{sAPP}\beta \rightarrow 0$
$\text{A}\beta_{42} \rightarrow 0$
$\text{A}\beta_{40} \rightarrow 0$

Notation: Reversible reaction ( $\leftrightarrow$ ); Irreversible reaction ( $\rightarrow$ ); Bound X and Y species are marked as a (X:Y), 0 on left side indicates zero order generation, 0 on the right side indicates first order clearance.

calibrated to match trends in ISF and CSF in reported results (Karelina et al., 2021; Geerts et al., 2023b). Note that to create the ROM, the higher order aggregates (o, O, F, and P) were treated as assemblies where the composite rate constants limit pure simplification into stoichiometric relationships.

The A $\beta$  aggregation model involves several additional steps observed in *in vitro* and preclinical models, such as plaque catalyzed secondary nucleation, fragmentation, dissociation of oligomers, protofibril breakup, protofibril and plaque growth saturation and microglia clearance. Individual steps of the A $\beta$  aggregation reaction mechanisms were formulated using published mechanisms (Scheidt et al., 2019; Rinauro et al., 2024; Niu et al., 2024) and the reference 25-step model (Geerts et al., 2023b). These main components were accounted for based on reaction mechanisms depicted in Figure 4B.

Note that M appears in Figure 4B in five boxes (1, 2, 3, 5, and 7) and the ODE for M includes four rate terms, R, and efflux, J, as shown in Equation 1 below:

$$\frac{dM}{dt} = R_{np} + R_{2n} + R_{pg} - R_{cl}^{IDE} + J_{B-b} \quad (1)$$

where  $R_{np}$  is the reversible nucleation-polymerization rate,  $R_{2n}$  is the secondary nucleation rate catalyzed by plaque (P),  $R_{pg}$  is the addition of monomers to oligomers and their conversion to plaque (P),  $R_{cl}^{IDE}$  is the microglia enzymatic degradation of soluble A $\beta$  (M), and  $J_{B-b}$  is the A $\beta$  (M) efflux rate by various transporters and fluid clearance between brain interstitial fluids (ISF) and body fluids.

The reversible nucleation-polymerization rate for monomer M binding to higher aggregates (D, o, O, F, P), Box 1 in Figure 4B is:

$$R_{np} = -2k_f^M M^2 + 2k_b^M D - k_f^D MD + k_b^D o - k_f^O Mo + k_b^O O - k_f^F MO + k_b^F P \quad (2)$$

Detailed rate kinetics and rate constants are provided in the Supplementary material. While nucleation of additional species is feasible, nucleation of monomers to multimers was selected in this work as the most energetically favorable option.

## 2.4 A $\beta$ transport and biodistribution in the whole-body model

The mAD model simulation of A $\beta$  biodistribution in the whole body was adapted from a whole body PBPK model topology originally developed for modeling antibodies targeting the central nervous system (CNS) (Bloomingdale et al., 2021). The A $\beta$  transport module spans the CNS compartments (brain vascular, BBB, BCSFB, ISF, CSF, and PVS) and the systemic compartments (plasma, lymph, tissue vascular, tissue barrier and tissues), as shown in Figure 5A. Flow assumptions are based on biodistribution principles of small molecules.

Small molecules and A $\beta$ -peptides distribute across body fluids (interstitial (ISF), cerebrospinal (CSF), perivascular spaces (PVS) and plasma) through convective and diffusive transport. While the blood-brain barrier (BBB) limits exchange between ISF and plasma, ISF and CSF are in direct fluid communication, enabling A $\beta$  exchange, including various soluble A $\beta$ -peptides (sA $\beta$ s), which are in constant equilibrium between the ISF and CSF (Mroczko et al., 2018; Schreiner et al., 2023; Teunissen et al., 2018). Within the ISF, diffusion and convection are comparable; however, in the CSF and PVS, convection dominates with drainage velocity on the order of  $8.3 \times 10^{-6}$  m/s (Rey and Sarntinoranont, 2018; Thomas, 2019). Although the convective transport rate for soluble molecules does not depend on the molecule size, the diffusive flux in the “porous” extracellular space is a strong function of the sA $\beta$  molecule size, shape, charge, tortuosity of pathway ( $\lambda \sim 1.6$  in ISF) and on the sA $\beta$  concentration gradient. We have used these property data to derive the size-independent Péclet numbers (Table 2), defined as the ratio of bulk fluid motion to the rate of diffusive transport between the ISF, PVS, and the lymph.

A schematic of the whole body biodistribution assumptions for diffusive and active transport is shown in Figure 5A. The “reaction”

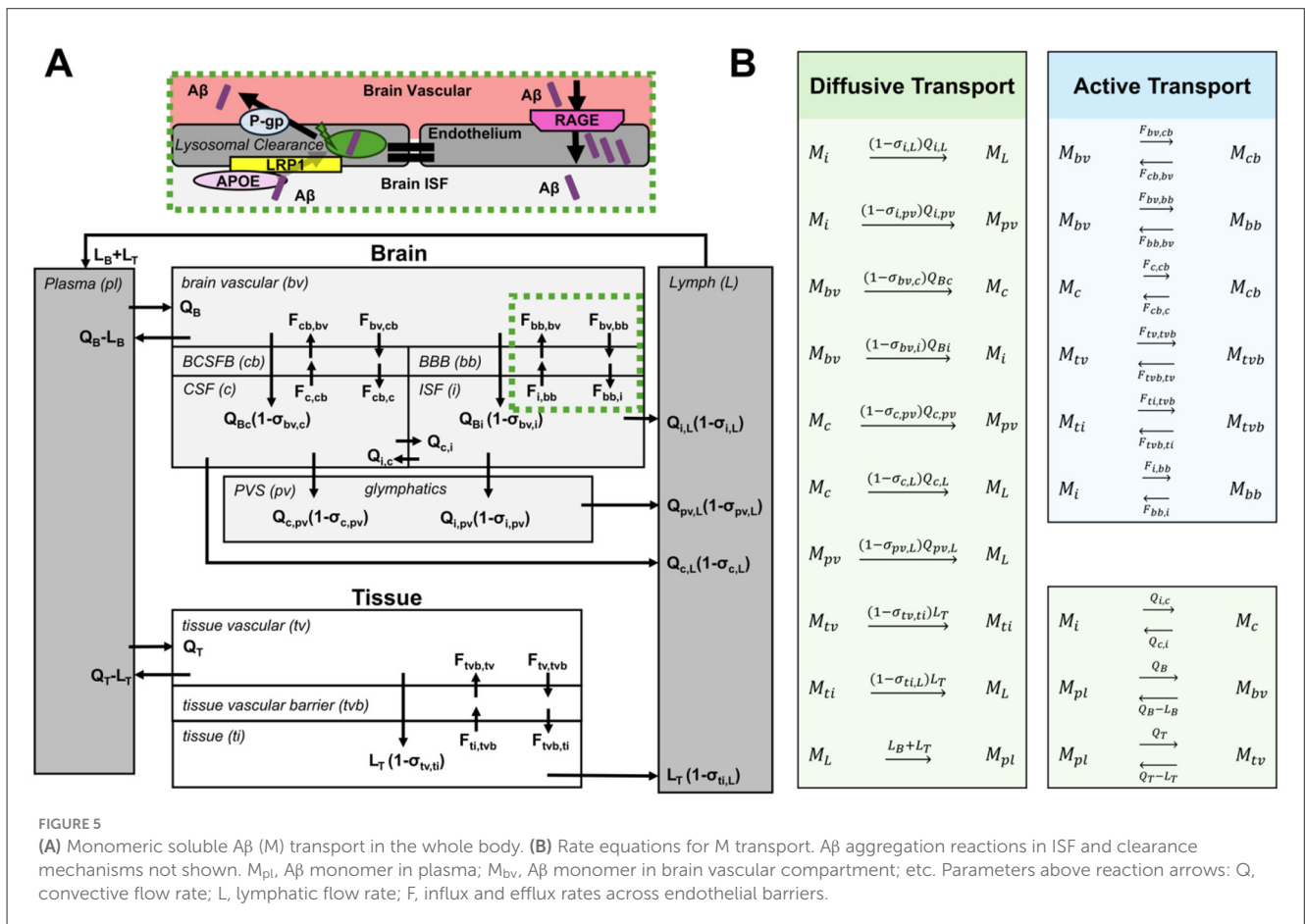
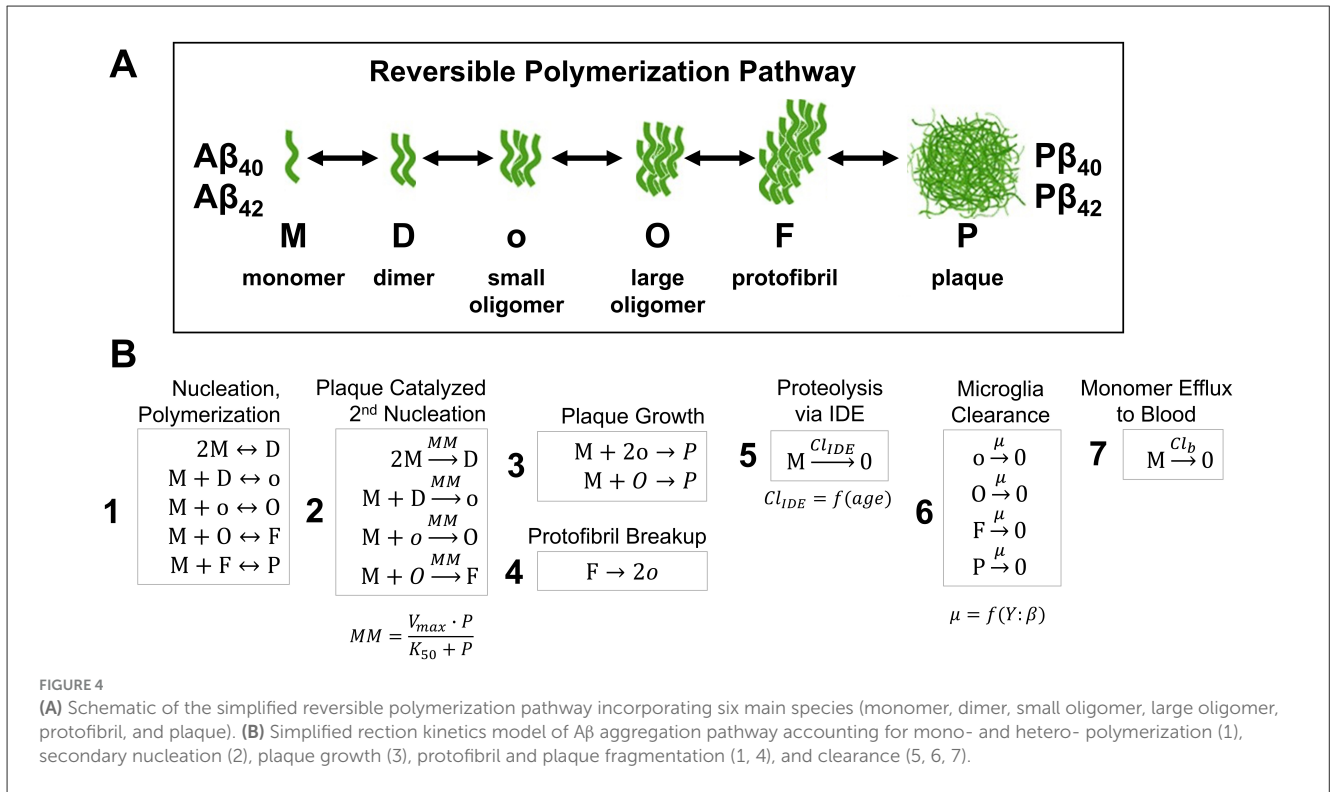


TABLE 2 Pécellet numbers for species diffusive transport of soluble A $\beta$  peptides.

Species	Pécellet numbers	
	$\sigma_{i,pv}$	$\sigma_{pv,L}$
M	0.200	0.650
D	0.900	0.900
o	0.900	0.900
O	0.990	0.990
F	0.999	0.999

mechanisms, shown in Figure 5B, are used by the CoBi ODE-Gen module to generate the corresponding ODEs. The model incorporates 11 compartments and therefore 11 ODEs are used to describe transport of each A $\beta$  peptide (A $\beta_{40}$ , A $\beta_{42}$ ). Detailed reaction kinetics and constants for A $\beta$  monomer (M) transport in the CNS compartments ( $M_{bv}$ ,  $M_{cb}$ ,  $M_{bb}$ ,  $M_i$ ,  $M_c$ ,  $M_{pv}$ ) and the systemic compartments ( $M_{pl}$ ,  $M_L$ ,  $M_{tv}$ ,  $M_{tvb}$ ,  $M_{fi}$ ) are provided in the Supplementary material. For simplicity, the schematic and rate equations are presented for a generic A $\beta$  peptide.

#### 2.4.1 A $\beta$ transport across brain barriers

In healthy subjects, A $\beta$  is produced and cleared from the brain at rates of 7.6% and 8.3% of total A $\beta$  per hour, respectively (Chai et al., 2020). In the late onset AD (LOAD), this clearance rate is reduced by approximately 30% (Mawuenyega et al., 2010). Impaired A $\beta$  clearance across the BBB endothelial cells plays a crucial role in the pathogenesis of AD. It has been reported that about 85% of all brain A $\beta$  clearance occurs through the BBB (Shibata et al., 2000) and that neurovascular dysfunction contributes to this impaired A $\beta$  clearance in AD. Therefore, the mAD model accounts for two A $\beta$  transport pathways across brain barriers: fluid permeation and active transporters of influx and efflux.

Fluid transport of A $\beta$  monomers across the BBB, facilitated by aquaporins, is driven by the flow rate across the BBB from brain vascular (bv) to brain interstitium (i),  $Q_{Bi}(1 - \sigma_{bv,i})$ , and across the BCSFB from brain vascular (bv) to brain CSF (c),  $Q_{Bc}(1 - \sigma_{bv,c})$ , where  $\sigma \in [0,1]$  is the nondimensional reflection coefficient, dependent on the barrier pore size and the size of the transported molecule;  $\sigma = 1$  means the barrier is not permeable to that molecule.  $Q_{Bi}$  and  $Q_{Bc}$  are water flow rates across the BBB and BCSFB respectively.

The other barrier pathway for A $\beta$  is facilitated by various influx and efflux transporters on the BBB and BCSFB. Low-density lipoprotein receptor related protein 1 (LRP1) and P-glycoprotein (P-gp) transporters control the A $\beta$  efflux from interstitium to vasculature, while the receptor for advanced glycation end-products (RAGE) transporter controls the A $\beta$  influx from vascular to interstitial space (Figure 5A). The above effects can be accounted for via representative fluxes, driven by “convective” transporting rate constants which account for the barrier surface area, level of expression of transporters and their binding/release properties for various A $\beta$  isoforms. In this work, we assumed a constant

value where A $\beta_{42}$  was assumed to be removed across the BBB at a slower rate than A $\beta_{40}$  (Bell, 2007; Deane et al., 2008). However, the extraction of A $\beta$  via LRP1 transporters may be declining with age and is dependent on APOE status, which should be considered in future model iterations. In the present model we solved for total plasma A $\beta$  and used the unbound fraction in plasma,  $f_{up}$ , in all A $\beta$  flux and clearance terms.

#### 2.4.2 A $\beta$ in perivascular space

Perivascular spaces (PVS) are CSF-filled areas surrounding cerebral blood vessels that become visible on MRI when enlarged due to aging, hypertension, or cognitive impairment (Perosa et al., 2022). PVS fluid transport, induced by cerebral arterial vessel pulsations is a substantial factor in the net clearance of A $\beta$  and was thus added to the mAD model. Dilated PVS is associated with blocked CSF bulk flow, reduced A $\beta$  clearance from the brain parenchyma, and a contributor to AD pathology (Wardlaw et al., 2020; Zhou et al., 2021; Hasegawa et al., 2022). As arteries stiffen with age, the amplitude of pulsations are reduced, and insoluble A $\beta$  accumulates in the PVS drainage pathways. Furthermore, enlarged PVS may be an indicator of AD progression and act as an early diagnostic marker. The present model accounts for glymphatic drainage of soluble A $\beta$  peptides (flow rates limited by Pécellet numbers in Table 2), while plaques accumulate in the PVS where they are cleared by macrophages.

### 2.5 Enzymatic and microglial clearance

Outside of the CNS, A $\beta$  monomers were assumed to degrade at a constant rate of  $1.9 \times 10^{-4}$ /s. Within the CNS, A $\beta$  was assumed to be degraded intracellularly in lysosomes of microglia and astrocytes and extracellularly by either secreted or membrane-bound proteases (Marr and Hafez, 2014). Of these, Neprilysin (NEP) and insulin-degrading enzyme (IDE) are the two major catabolic enzymes that degrade A $\beta$  peptides. Both proteases decrease with age and show decreased expression in AD, especially in regions with high A $\beta$  loads, such as the hippocampus (Loeffler, 2023). Therefore, in our model, the A $\beta$  monomer protease degradation mechanism is represented by a Hill kinetics term with A $\beta$  monomer as a ligand and the maximum reaction velocity was assumed to decrease as a function of the patient’s age.

Microglia, the brain’s resident innate immune cells, clear pathological proteins and prune excess neuronal synapses from the CNS. In AD, oligomeric A $\beta$  bind to synapses which triggers microglial activation, contributing to excessive elimination of synapses and cognitive deficits. Normally, microglia exist in a quiescent state but can be activated by surrounding stimuli such as cellular debris and A $\beta$  agglomerates. This activation process involves microglial proliferation, increased secretion of inflammatory factors, cell surface receptor expression, and morphological changes. The early activation of microglia into the M2 phenotype that attempts to clear A $\beta$  is considered neuroprotective and anti-inflammatory. Compared to resting state, M2-polarized microglia show enhanced phagocytosis. However, with the development of the AD pathology, the M2 phenotype may

become dysfunctional over time and be replaced by the microglia M1 phenotype. M1-polarized microglia are pro-inflammatory and lose their phagocytosis capabilities (Wang et al., 2021; Guo et al., 2022).

Microglia interact with soluble and insoluble/fibrillar A $\beta$  forms. The present model accounts for these mechanisms by assuming that soluble A $\beta$  monomers (M) are degraded enzymatically by various proteases, such as NEP and IDE (Box 5 of Figure 4B), defined using Hill kinetic equations and assumptions in the Supplementary material.

All higher-order insoluble A $\beta$  agglomerate forms (o, O, F, P) were assumed to undergo microglial-dependent clearance in the ISF (Box 6 of Figure 4B). The clearance rate ( $k_{g,cl}^i$ ) of insoluble A $\beta$  forms (o, O, F and P) is expressed in Equation 3.

$$k_{g,cl}^i = \mu(t) \left[ fr(t) V_i^{high} + (1 - fr(t)) V_i^{low} \right] \quad (3)$$

Where  $\mu(t)$  is the normalized microglia density,  $fr(t)$  is the microglia phenotype fraction (varies between 0 and 1). At steady state,  $\mu(t)$  was assumed to be 1 and  $fr(t)$  was assumed to be 0.03 (close to zero).  $V_i^{high}$  for the healthy controls and  $V_i^{low}$  for AD subjects are the high and low clearance rate for specific A $\beta$  forms. We assumed that oligomers and protofibrils had the same clearance rate, but plaque clearance rate was 50% lower due to its insoluble more compact nature. These assumptions were adapted from Geerts et al. (2023b). Soluble and insoluble concentrations were modeled in the brain ISF and validated against experimental datasets reported in Karelina et al. (2017).

## 2.6 Risk factors

Family history and genetics are strong risk factors for AD. Late-onset AD (LOAD) is a polygenic disorder associated with at least 50 genes, of which the apolipoprotein E (APOE)  $\epsilon 4$  allele is the strongest risk factor (Yu et al., 2021). In humans, APOE is expressed as  $\epsilon 2$ ,  $\epsilon 3$  and  $\epsilon 4$  isoforms with frequency of 8%, 78% and 14%, respectively (Schipper, 2011). APOE lipoproteins bind to several cell-surface receptors and hydrophobic A $\beta$  peptides. The exact mechanism by which APOE isoforms increase/decrease AD risk is not fully understood, but APOE isoforms differently affect brain homeostasis and neuroinflammation, BBB permeability, glial function, synaptogenesis, oral/gut microbiota, neural networks, A $\beta$  clearance, and tau-mediated neurodegeneration. It has been generally accepted that APOE  $\epsilon 4$  decreases A $\beta$  clearance, increases aggregation and amyloid seeding without affecting A $\beta$  production. On the other hand, the APOE  $\epsilon 2$  allele is the strongest genetic protective factor (Hampel et al., 2020). Expression of various APOE alleles directly affects the risk of AD (Fernández-Calle et al., 2022).

In our model we account for APOE effects by multiplying the microglial clearance rate ( $k_{g,cl}^i$ ) in Equation 3 by a factor  $(1-\alpha)$ , controlling the kinetic rate constant of microglia clearance of individual A $\beta$  isoforms and agglomerates. We established a baseline value  $\alpha = 0$  for APOE non-carriers (APOE-) and  $\alpha > 0$  for APOE carriers (APOE+). For APOE carriers,  $\alpha$  was assumed to range from  $-0.02$  to  $1$ , and groups were stratified by APOE genotype and sex. These stratified APOE AD risk factors are aligned with recent clinical findings based on male/female population clinical

data (Chai et al., 2021). Homozygous ( $\epsilon 4$  and  $\epsilon 4$ ) carriers had the greatest increase in risk [12 x (men), 15 x (women)], heterozygous ( $\epsilon 4$  and  $\epsilon 3$ ) carriers had a mild increase in risk [3 x (men), 3.5–4 x (women)], and APOE  $\epsilon 2$  carriers have a slightly reduced risk [0.7 x (both sexes)].

## 2.7 Validation of the AD progression model using SUVR imaging data

Positron emission tomography (PET) imaging can be conducted to evaluate AD progression in patient populations. Cerebral amyloid loads are quantified by administration of radioligands, which bind to amyloid fibrils and plaques at brain synapses. The radioactivity concentrations throughout the brain are quantified in terms of the Standardized Uptake Value Ratio (SUVR) between the target and reference brain tissue regions, shown in Equation 4.

$$SUVR = \frac{\text{Uptake in Target Region}}{\text{Uptake in Reference Region}} \quad (4)$$

The cerebellum is commonly used as a reference region because it is notably free from fibrillar A $\beta$  in sporadic AD and a majority of neurons are granule cells with only a handful of synapses, compared to cortical neurons which may host tens of thousands of synapses (Lyo et al., 2015). Equation 5 was formulated to calculate the SUVR using computed A $\beta$  load. The A $\beta$  load ( $\beta_L$ ) was calculated as a weighted sum of individual A $\beta$  agglomerates (o, O, F, P) for A $\beta_{40}$ , A $\beta_{42}$  in Equation 6.

$$SUVR = C_0 + \frac{C_1 \beta_L^{C_2}}{C_3^{C_2} + \beta_L^{C_2}} \quad (5)$$

$$\beta_L = \beta^o + \beta^O + \beta^F + C_4 \beta^P \quad (6)$$

where calibrated constants  $C_0 = 1.0$  (fixed),  $C_1 = 4.65$ ,  $C_2 = 3.3$ ,  $C_3 = 630,000$ , and  $C_4 = 1.95$ . Note that  $C_4 > 1$  indicates that the PET tracer has higher affinity for plaques compared to other agglomerates. Calculated SUVR was then validated against clinical data of aging healthy individuals and in amyloid positive subjects (Jack et al., 2013a).

## 3 Results

### 3.1 A $\beta_{40}$ , A $\beta_{42}$ generation, and aggregation

APP processing and subsequent generation of A $\beta$  peptides through the amyloidogenic pathway was implemented in the CoBi framework based on the model developed by Madrasi et al. (2021) and outputs were replicated. The 25-variable A $\beta$  aggregation model defined in Geerts et al. (2023b) was then replicated in CoBi and reduced to a 6-variable reduced order model (ROM) of A $\beta$  aggregation. Assumptions and model parameters for monomers and dimers were unchanged and resulting concentration profiles for A $\beta_{40}$  and A $\beta_{42}$  in the isolated brain ISF compartment were compared between the 6-variable mAD model and the 25-variable Geerts model (Figure 6). The average percent difference between

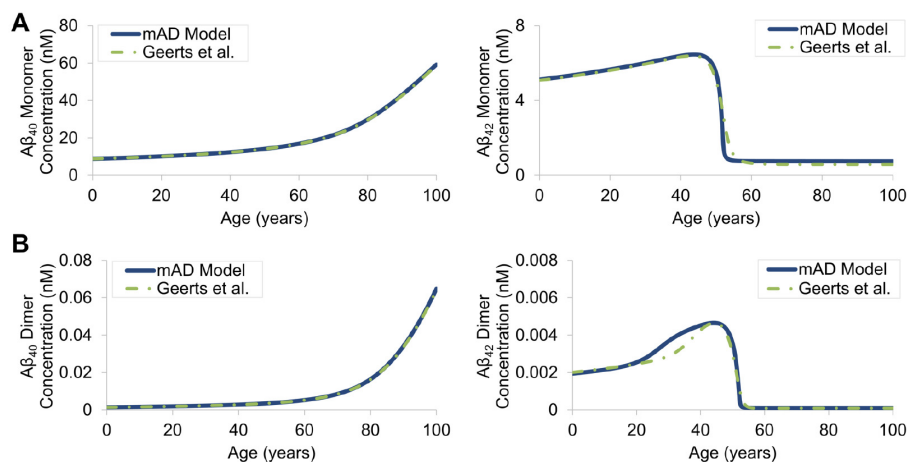


FIGURE 6

Simulated  $A\beta_{40}$  and  $A\beta_{42}$  monomer (A) and dimer (B) concentrations comparing the developed ROM  $A\beta$  agglomeration outputs in the isolated brain ISF from the mAD model to outputs from the higher-order Geerts et al. (2023b) model.

models was 0.36% for  $A\beta_{40}$  monomers and 0.45% for  $A\beta_{40}$  dimers, demonstrating excellent agreement. The average percent difference between the mAD model and the Geerts model was 14.29% for  $A\beta_{42}$  monomers and 17.91% for  $A\beta_{42}$  dimers. Greater deviation in  $A\beta_{42}$  predictions is due to greater effect of the higher order species on  $A\beta_{42}$  agglomeration cascades. Direct comparison between outputs for higher-order agglomerates was not feasible as it was difficult to establish correlation between present “lumped” species (o,O,E,P) and individual components of the 25-species reference model. Nevertheless, monomer and dimer profile agreements provided sufficient confidence for integration of  $A\beta$  generation and aggregation terms with full body transport and further validation.

### 3.2 $A\beta$ transport and biodistribution

$A\beta$  transport and distribution accuracy relies on accuracy of transport from the brain ISF, which is where  $A\beta$  generation and aggregation were assumed to occur. Simulations in the mAD model compared the effect of accumulated insoluble  $A\beta_{42}$  in the brain ISF over time (Figure 7A) vs. soluble  $A\beta_{42}$  (Figure 7B). Insoluble concentrations increased to orders of magnitude greater than soluble concentrations, which adequately simulates how soluble, toxic  $A\beta$  peptides aggregate into insoluble forms. Compared to the clinical data, reported by Karelina et al. (2017), the model effectively captures concentrations of soluble and insoluble concentrations of  $A\beta_{42}$  in the ISF of the AD brain between the ages of 70–80 years old.

### 3.3 Validation of the AD progression model using SUVR imaging data

The mAD model was validated against clinical data of aging healthy individuals and in amyloid positive subjects. In Jack

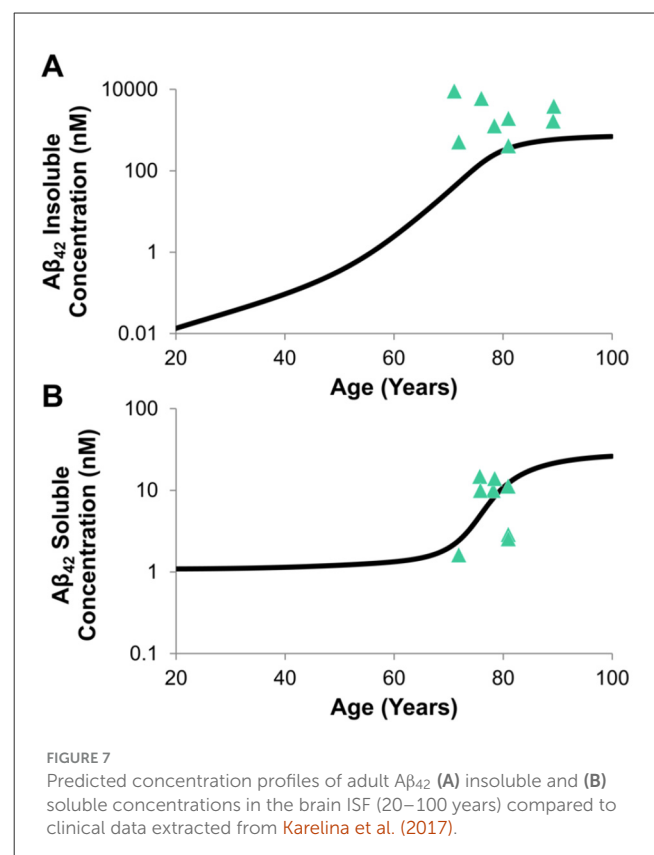


FIGURE 7

Predicted concentration profiles of adult  $A\beta_{42}$  (A) insoluble and (B) soluble concentrations in the brain ISF (20–100 years) compared to clinical data extracted from Karelina et al. (2017).

et al. (2013a), an SUVR profile of the temporal trajectory of  $\beta$ -amyloid accumulation was generated from 260 participants 70–92 years old. Because clinical data are typically collected from elderly populations with amyloid present, the current model can be used to computationally “extrapolate” the SUVR status not only into the future but also for the prodromal stage. As shown in Figure 8A, based on the fit of the initial clinical SUVR data

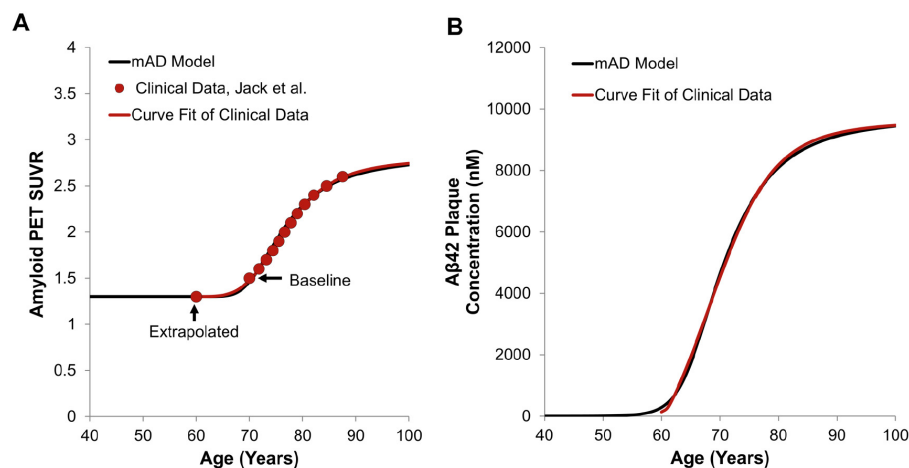


FIGURE 8

(A) Generation of the sigmoid function fit to clinical data, including an extra data point extrapolated to the age of 60. The baseline SUVR was set to 1.5 at the age of 70. (B) Comparison of brain  $A\beta_{42}$  plaque formation in a human subject obtained with the current AD progression model and the curve fit of the clinical data. Clinical data was extracted from Jack et al. (2013a).

collected, we extrapolated the SUVR back into a prodromal baseline state at age 60. The clinically observed SUVR was then correlated to  $A\beta_{42}$  plaque profiles in the brain ISF and compared to the predicted  $A\beta_{42}$  plaque concentrations from the mAD progression model (Figure 8B). This computational capability correlating the clinical SUVR and various brain  $A\beta$  agglomerates (o, O, F, P) could be a useful tool to correlate medical imaging and body fluid biomarkers data.

### 3.4 Simulation of APOE risk factors

The full aggregation model described by Geerts et al. accounts for APOE carriers/non-carriers without distinction between various APOE alleles ( $\epsilon 4$ ,  $\epsilon 3$ ,  $\epsilon 2$ , and their combinations) (Geerts et al., 2023b). The mAD model incorporates the simulated effect of APOE alleles on  $A\beta_{42}$  plaque concentrations in the brain ISF, however, only the effects of  $\epsilon 3$  and  $\epsilon 4$  alleles were demonstrated in this report. Kinetic parameters controlling the effect of APOE on various  $A\beta$  profiles were identified during APOE model calibration. Simulation of the effect of APOE kinetic parameters on profiles of  $A\beta_{42}$  plaque in the ISF demonstrated accelerated accumulation of  $A\beta_{42}$  plaques in the ISF up to 5 years earlier compared to non-carriers (Figure 9). A limitation of the current model is that it does not directly account for risk factors associated with specific  $\epsilon 2$ ,  $\epsilon 3$ , and  $\epsilon 4$  APOE isoforms and only accounts for different microglial clearance rates. In the future, this capability could be adapted to account for risk factors for all APOE alleles ( $\epsilon 4$ ,  $\epsilon 3$ ,  $\epsilon 2$ , and their combinations) in the model.

Time profiles of  $A\beta_{42}$  species (M, O, F, P) in the brain ISF was simulated in APOE carriers and non-carriers (Figure 10). As expected, APOE carriers with  $\epsilon 3$  and/or  $\epsilon 4$  alleles have accelerated agglomeration processes causing earlier development of AD. Once the insoluble species starts forming, such as oligomers and protofibrils, the enzymatic degradation by microglial cells is less effective with age. This is demonstrated by the lack of

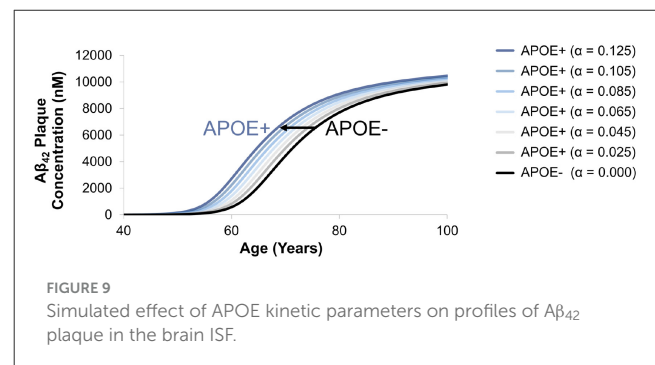


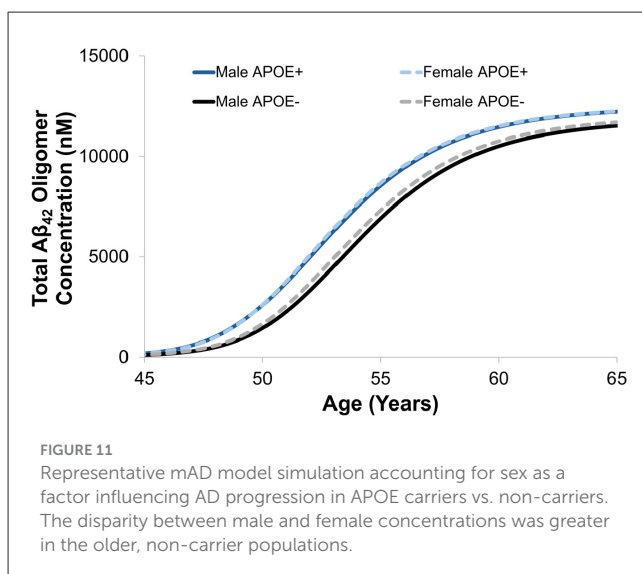
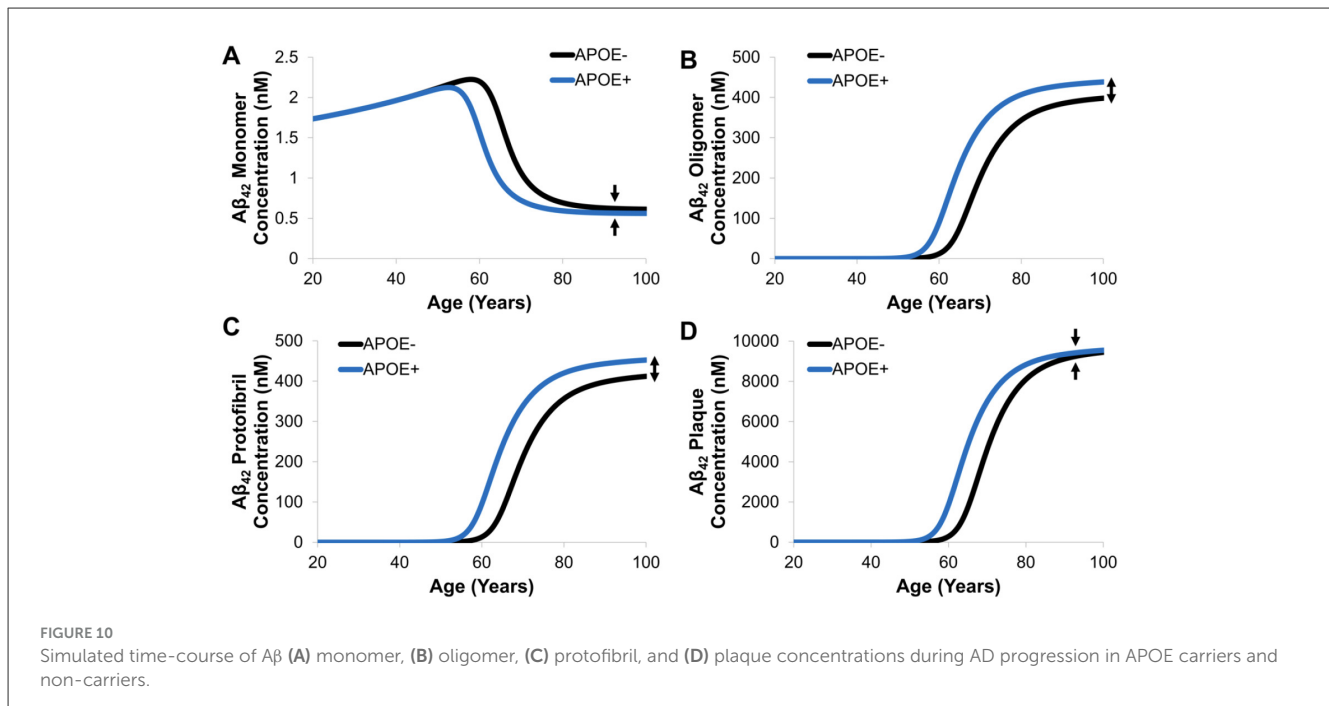
FIGURE 9

Simulated effect of APOE kinetic parameters on profiles of  $A\beta_{42}$  plaque in the brain ISF.

convergence of oligomer and protofibril concentrations between 80 to 100 years of age. On the other hand, once the plaque is formed, APOE has less of an effect on microglial clearance and the concentration of  $A\beta_{42}$  plaque converges. This observation could be important for understanding toxicity of intermediate species where recent evidence shows that the heterogeneous nature of oligomers contributes substantially to neurotoxicity and resulting neurodegeneration (Tolar et al., 2024, 2021). The mAD model also demonstrates the effect of sex on  $A\beta$  dynamics in the presence or absence of APOE alleles. In general, females had slightly higher concentrations of  $A\beta$  compared to males and the discrepancies between male and female-predicted concentrations was greater in the non-carrier group (Figure 11).

## 4 Discussion

The high complexity of AD pathophysiology and disappointing results of clinical trials of various drug candidates call for better understanding of the disease using systems biology-based, multiscale and multidisciplinary modeling approaches (Hampel et al., 2018; Uleman et al., 2024). Development of clinically



relevant computational models of disease progression, diagnostics and medical treatment is a monumental task, which will require progress in and contributions from various disciplines of medicine, systems biology, biochemistry, pharmacology, physics, computing, neuro-diagnostics, cognitive physiology and others. While reported computational models have advanced the understanding of AD mechanisms, several limitations impact their clinical utility (Moravveji et al., 2024; Paul et al., 2025; Chamberland et al., 2024). Such models typically require simplifications to make complex biological processes computationally feasible and/or involve many parameters which must be either estimated to achieve desired trends in simulation results or calibrated using clinical data. As in all mathematical models of neuro-physiological processes, the

most difficult task is to demonstrate quantitative model validation against relevant clinical data.

This paper describes a mechanistic model of AD progression integrating the brain synaptic-interstitial scale models of A $\beta$  generation and agglomeration, formation and detection of amyloid plaques, and the whole-body biomarker kinetics (BxK) of A $\beta$  isoforms. It is constructed based on previously reported models of APP processing and A $\beta$  generation (Madras et al., 2021), the A $\beta$  agglomeration cascade (Geerts et al., 2023b), and a whole-body physiologically-based pharmacokinetic (PBPK) model (Bloomingdale et al., 2021) adapted to simulate A $\beta$  biomarker kinetics (BxK). Various components of the integrated AD progression model were verified against the reference models and compared to available clinical data. Combination of these mechanistic processes into a single model and demonstration of the preserved dynamics, shown in this work, substantially broadens the applications of the original model components. Although other frameworks may exist with these components, the methods described in this manuscript take a unique approach toward adapting, combining, and interpreting these mechanistic processes to both improve computational efficiency (reduced order modeling of aggregation pathways) and extend complexity (i.e., incorporating the perivascular space, reaction kinetics of the non-amyloidogenic pathway, etc.). Further refinement of these features and processes is anticipated to improve understanding of disease progression and optimization of intervention strategies.

The reduced order model of A $\beta$  generation and agglomeration kinetics accurately predicted the temporal variations of A $\beta_{40}$  and A $\beta_{42}$  and compared well with monomer and dimer concentrations (Figure 6) obtained using the full Geerts pathway model (Geerts et al., 2023b). Aggregation model assumptions and systems transport from the brain ISF was further validated through comparison of time-dependent concentrations of soluble and insoluble A $\beta_{42}$  in the brain ISF with clinical data reported in

Karelina et al. (2017). High confidence in profile shape and concentrations justifies the assumptions for transport and clearance (Figure 7). Studies have indicated that aggregation of soluble A $\beta$  can occur as a neuroprotective mechanism to pathogens or breaches in the BBB, which then develops into insoluble forms that are never properly cleared (Sehar et al., 2022; Brothers et al., 2018). Therefore, increased brain concentrations of soluble A $\beta$  is known to be a good indicator of early disease onset where therapeutic approaches have been developed to improve clearance of these molecules and reduce overall toxicity (Tolar et al., 2024).

One major advantage of the mAD model is its endothelial barrier endosomal processing paths that could be used for PBPK modeling of amyloid targeting biologics. The PBPK model that was adapted in this work was intentionally selected for integration with the mAD model due to its demonstrated use for the prediction of anti-amyloid drugs (i.e. lecanemab, aducanumab, and donanemab) (Geerts et al., 2023b, 2024b). This framework has also been shown to be easily adapted for multiple drug classes (Bloomingdale et al., 2021, 2022; Geerts et al., 2023a). In addition to anti-amyloid therapies, the mAD model has applications for simulating the effects of anti-inflammatory modulators, aggregation inhibitors, and gene therapies. Generally, anti-inflammatory therapies work by reducing microglial activation and associated secretase activity (Vom Hofe et al., 2025; Sastre and Gentleman, 2010; Chu et al., 2024). Aggregation inhibitors function to block A $\beta$  and tau from clumping, disrupt existing fibrils, or promote their clearance (Nam et al., 2025). Lastly, gene therapies use viral or non-viral vectors to deliver genes that will combat the detrimental effects of AD, such as introducing APOE  $\epsilon$ 2 allele to elicit a protective factor and combat the effects of APOE  $\epsilon$ 4 (Doshi et al., 2024). Therefore, implementation of the mAD model to predict efficacy of anti-amyloid, anti-inflammatory, and non-amyloid therapies could greatly advance therapeutic development for AD.

In addition to the therapeutic advantages of the mAD model, use of the BxK transport model to simulate effects of mechanistic changes in transvascular clearance could be extremely valuable. The current model assumes a constant rate of A $\beta$  transport across the BBB for each peptide. However, expression of LRP1 and P-gp are known to be affected by age, genetics, APOE presence, disease progression, and disease pathology (Kanekiyo et al., 2012; Chai et al., 2020; Chiu et al., 2015; Erdo and Krajcsi, 2019). Reduced expression of LRP1 and/or P-gp impairs the removal of A $\beta$  from the brain, which accelerates A $\beta$  accumulation (Shinohara et al., 2017) and propagates the disease state at the BBB (Nicolas, 2015). To advance the mAD model further, the rate constants for A $\beta$  BBB transport by LRP1, P-gp, and RAGE could be expressed as age-dependent correlations, for which relevant clinical data would be required.

Validation of rate of plaque formation and concentration was performed using an extrapolation method from SUVR *in vivo* clinical data, which demonstrated effective correlation of model results to imaging data (Figure 8), strengthening the translational capabilities of the mAD model. A simple semi-empirical model of the amyloid plaque buildup has been used to calculate temporal SUVR for specific PET ligands. As access to larger population datasets improves, SUVR methods could be expanded in future iterations to calibrate effects of risk factors on plaque formation.

In the case of validating model predictions for interventional studies, modeling of Amyloid-Related Imaging Abnormalities-Edema (ARIA-E), a side effect of anti-amyloid drugs for Alzheimer's, could be incorporated into the mAD framework to guide patient safety and treatment. Modeling and validation of ARIA-E incidence in response to therapeutic administration has been previously conducted in combination with QSP models (Geerts et al., 2024b) and should be adapted to account for APOE genotypes/other risk factors (Majid et al., 2024). Incorporation of ARIA-E modeling for specific pathologies and therapeutic strategies would provide a powerful tool to optimize clinical trials and accelerate market acceptance.

Longitudinal biomarker studies reveal that the latent phase of AD precedes the onset of symptoms by decades (Barthélemy et al., 2020; Rafi and Aisen, 2023). Once patients reach the dementia stage, existing treatments have minimal impact on their functional activities and quality of life. Thus, there is a growing interest in developing biomarkers that could be used to detect these changes in the brains of at-risk individuals to enable earlier diagnosis and interventions. Rapid advancements in neuroimaging, genome sequencing and novel immunoassays provide the opportunity for accurate quantification of and correlation between intracranial and body fluid biomarkers. Computational models of linked neurobiology of AD progression and the whole body BxK described in this study will facilitate back-translation of noninvasively detected blood-based biomarkers to preceding intracranial neurodegenerative pathways responsible for generation and release of those biomarkers. This, in turn, can guide additional diagnostics, optimize timing of therapeutic interventions, enable biomarker-guided targeted therapies, and assess the treatment efficacy, and early detection of adverse reactions (Aisen et al., 2022; Fan and Wang, 2020; van der Flier et al., 2023).

Progression from normal cognition (NC) to mild cognitive impairment (MCI) and into dementia depends on a range of risk factors. It has been demonstrated that cognitive symptoms fluctuate between NC and MCI and may be potentially reversible (Shimada et al., 2019; Qin et al., 2023; Sanz-Blasco et al., 2022). Identifying individuals with MCI that could benefit from early interventions could have immense health implications. Potentially modifiable (cardiovascular, addictions, obesity, sleep, educational level, inflammation) and non-modifiable (age, genetic, family history of dementia, gender, APOE $\epsilon$ 4, brain injuries) risk factors that affect the disease development and progression have been identified (Jones et al., 2024). Population studies suggest that over 40% of dementia cases may be prevented or delayed by addressing modifiable risk factors. We contend that mechanistic models of MCI-AD progression, accounting for both types of risk factors could support medical intervention decisions in the not-so-distant future. At present, our model explicitly accounts for age as a risk factor as well as APOE presence/allele combinations as a function of microglial clearance. However, additional components of the current model could be adapted to account for other risk factors.

Risk factor assessment in the mAD model demonstrated earlier accumulation of plaques by approximately 5 years for APOE carriers ( $\epsilon$ 3 and/or  $\epsilon$ 4 alleles only). Another interesting feature shown in the effect of APOE on oligomer and protofibril

concentrations was an observable lack of convergence between 80 and 100 years old, which may correlate to the increased toxicity of intermediate species. The effect of sex as a risk factor of AD was also accounted for where females showed an earlier accumulation of oligomers compared to males. The model only accounts for this as a linear effect, however, the onset of menopause and effects in aging women were not accounted for and may not have a linear effect on A $\beta$  concentrations. These relationships can be further calibrated and validated based on experimental datasets to better associate risk factors with amyloid cascades.

This mAD model was recently adapted as a diagnostic tool used to predict A $\beta$  monomer concentrations in blood serum following cumulative blast exposure in military personnel. In the blast biomarker model, the rate of APP synthesis was assumed to increase proportional to the blast overpressure. Simulations predicted A $\beta$ <sub>42</sub> levels within 7% error on average, validated based on a population of fifteen service members undergoing weapons training (Norris et al., 2025). These strong acute predictions in A $\beta$  kinetics could merge with the mAD model to identify at-risk populations or improve mechanistic understanding of TBI-related dementia in addition to AD (Belding et al., 2024; Mendez, 2017). Altogether, this model framework demonstrates immense potential to transform diagnostic, prognostic, and therapeutic strategies to support life-long neurological health.

The mechanistic formulation of the present model provides an excellent foundation for incorporation of models of effects of other risk factors affecting the disease development and progression. We demonstrated an approach to account for how APOE allele combinations would affect microglial clearance. Work is ongoing to refine our brain injury risk factors (Norris et al., 2025), gender (male vs. female) risk factors, and the refinement of the APOE risk factor model accounting for heterozygous and homozygous male and female carriers of  $\epsilon$ 4,  $\epsilon$ 3 and  $\epsilon$ 2 isoforms. Altogether, the developed mAD model was constructed for easy adaptation into neuroscience QSP frameworks, which is expected to expand capabilities for modeling small molecules and immunotherapies targeting various MCI and AD development, as well as progression pathways.

## 4.1 Model limitations and future refinements

Construction of the mAD model by adaptation and integration of previously developed models takes on the limitations inherent in the original models (Madrasi et al., 2021; Bloomingdale et al., 2021; Geerts et al., 2023b). A few suggestions for future refinement of the mAD model are provided below.

*The APP processing model neglects the intra-neuronal paths of APP synthesis, transport and recycling.* The mAD model only accounts for a singular rate of APP synthesis and peptide generation into the ISF. However, within the neuron, APP can be distributed throughout the axonal and somatodendritic domains and peptides are not always cleaved at the synapse (Wang et al., 2024). As more information about APP processing phenotypes of AD arise, the effect of AD on the spatiotemporal regulation

of APP trafficking and location(s) of APP processing in human neurons should be accounted for in these models. Further, while the mAD model accounts for both the amyloidogenic and non-amyloidogenic pathways, only the former has been elaborated and partially validated. Future calibration of the non-amyloidogenic pathway could be performed through comparison of published concentrations of the p3 peptide (known to develop its own aggregates), which may be important for analyzing downstream effects of APP processing (Kuhn et al., 2020).

*A $\beta$ <sub>40</sub> and A $\beta$ <sub>42</sub> agglomeration was assumed to occur independently and form homogeneous aggregates.* This assumption was inherently defined by incorporation of the Geerts et al. (2023b) model. However, A $\beta$  plaques can have different morphologies and compositions depending on the AD etiology (Koutarapu et al., 2025). Co-aggregation and off-pathway aggregation of the two isoforms can also occur (Li et al., 2023; Oren et al., 2021), further indicating that etiology-specific agglomeration cascades may be developed as population data arises to better support assumptions for plaque composition. Additionally, simplification of the agglomeration cascade to only six species limits the ability of the mAD model to investigate the effects of intermediate products (i.e. trimers  $\rightarrow$  large oligomers) on AD progression without further validation.

*A relatively simple model of neuroinflammation caused by accumulation of higher-level A $\beta$  aggregates was postulated.* A recent study showed that a majority of the published models of neuroinflammation were developed in the context of understanding AD, as opposed to other neurodegenerative diseases (Foster-Powell et al., 2025). Further, the complexity of these models continues to expand to include microglia, astrocyte, and t-cell interactions as well as pro-inflammatory cytokines. Receptor binding and transcription factor integration was also proposed as a future direction for AD modeling based on common cancer models (Foster-Powell et al., 2025). Development of more complex neuroinflammation/inflammasome models influencing amyloid aggregation could be important for investigation of mechanistic factors leading to AD and related dementias, such as traumatic brain injury-related dementia.

*The current model assumes that all APP/A $\beta$  pathways occur in a homogeneous brain space.* There are two problems with that. First, this does not account for the role of peripheral amyloid peptide generation and aggregation. Over 90% of A $\beta$  peptides found in the circulating blood are platelet-derived and AD is known to effect metabolism of platelet-derived A $\beta$  (Fu et al., 2023) and aggregation outside of the CNS (Gamez and Morales, 2025; Shi et al., 2024). Second, the model represents the CNS volume by only six sub compartments (vascular, BBB, BCSFB, ISF, CSF and PVS), which does not account for spatial effects of A $\beta$  pathology within the AD brain. Distinct patterns of A $\beta$  deposition can occur depending on different clinical phenotypes, which may be important to consider when developing diagnostic and prognostic models (Lecy et al., 2024). As CoBi tools enable multiscale, multiphysics simulations (Przekwas et al., 2006), the single brain compartment can be split into anatomically distributed regions with variable disease progression rates observed in neuroimaging. Nevertheless, the AD progression model provides a good foundation for future refinement.

The rate of A $\beta$  transport across the BBB was assumed to be constant. However, A $\beta$  efflux is known to be affected by APOE protein isoforms ( $\epsilon$ 2,  $\epsilon$ 3,  $\epsilon$ 4), which bind to LRP1 with different affinities. LRP1 can bind not only A $\beta$  but also APOE and A $\beta$ :APOE complexes. The impaired binding of APOE $\epsilon$ 4 can lead to reduced clearance efficiency of A $\beta$ , enhancing AD pathology. Moreover, APOE $\epsilon$ 2/A $\beta$  and APOE $\epsilon$ 3/A $\beta$  complexes are cleared at the BBB via LRP1 at a substantially faster rate than APOE $\epsilon$ 4/A $\beta$  complexes (Kanekiyo et al., 2014; Belaidi et al., 2025). Such considerations should be implemented in future model iterations.

Development of AD pathology involves not only formation of A $\beta$  plaques but also growth of intracellular neurofibrillary tangles containing hyper-phosphorylated Tau. Abnormal phosphorylation of Tau can lead to aggregation of Tau fibrils in a similar fashion to A $\beta$  peptides, leading to neurofibrillary tangles (NFTs) where much of the developed framework reported here can be applied to modeling NFT formation. Implementation of a Tau pathology model coupled to the existing A $\beta$  model could help improve accuracy of AD progression predictions. Further, prediction of Tau pathology in the context of AD can also enable estimation of the pathological burden of other tauopathies contributing to cognitive and behavioral deficits (Granholm and Hamlett, 2024).

Robust clinical validation is necessary to strengthen predictive capabilities of this tool. This study performs validation of A $\beta$ <sub>42</sub> concentrations in the brain ISF. Improved access to larger datasets is required for validation of the mAD model predictions in the CSF, blood, and other tissues as well as validation of additional amyloidogenic and non-amyloidogenic species.

## Data availability statement

The original contributions presented in the study are included in the article/Supplementary material. Further inquiries can be directed to the corresponding author.

## Author contributions

AP: Conceptualization, Methodology, Validation, Visualization, Writing – original draft, Writing – review & editing. CN: Software, Validation, Visualization, Writing – review & editing. HG: Software, Writing – review & editing, Conceptualization, Project administration, Supervision.

## References

- Aisen, P. S., Jimenez-Maggiora, G. A., Rafii, M. S., Walter, S., and Raman, R. (2022). Early-stage Alzheimer disease: getting trial-ready. *Nat. Rev. Neurol.* 18, 389–399. doi: 10.1038/s41582-022-00645-6
- Allwright, M., Mundell, H. D., McCorkindale, A. N., Lindley, R. I., Austin, P. J., Guennewig, B., et al. (2023). Ranking the risk factors for Alzheimer's disease; findings from the UK Biobank study. *Aging Brain* 3:100081. doi: 10.1016/j.nbas.2023.100081
- Barthélemy, N. R., Li, Y., Joseph-Mathurin, N., Gordon, B. A., Hassenstab, J., Benzinger, T. L., et al. (2020). A soluble phosphorylated tau signature links tau, amyloid and the evolution of stages of dominantly inherited Alzheimer's disease. *Nat. Med.* 26, 398–407. doi: 10.1038/s41591-020-0781-z
- Belaidi, A. A., Bush, A. I., and Ayton, S. (2025). Apolipoprotein E in Alzheimer's disease: molecular insights and therapeutic opportunities. *Mol. Neurodegener.* 20:47. doi: 10.1186/s13024-025-00843-y
- Belding, J. N., Bonkowski, J., Englert, R., Grimes Stanfill, A., and Tsao, J. W. (2024). Associations between concussion and more severe TBIs, mild cognitive impairment, and early-onset dementia among military retirees over 40 years. *Front. Neurol.* 15:1442715. doi: 10.3389/fneur.2024.1442715

## Funding

The author(s) declared that financial support was not received for this work and/or its publication.

## Acknowledgments

The authors would like to express gratitude to the late ZJ Chen at CFD Research Corporation for his contribution to the development of the mAD Model described in this work.

## Conflict of interest

AP, CN, and HG were employed by CFD Research Corporation.

## Generative AI statement

The author(s) declared that generative AI was not used in the creation of this manuscript.

Any alternative text (alt text) provided alongside figures in this article has been generated by Frontiers with the support of artificial intelligence and reasonable efforts have been made to ensure accuracy, including review by the authors wherever possible. If you identify any issues, please contact us.

## Publisher's note

All claims expressed in this article are solely those of the authors and do not necessarily represent those of their affiliated organizations, or those of the publisher, the editors and the reviewers. Any product that may be evaluated in this article, or claim that may be made by its manufacturer, is not guaranteed or endorsed by the publisher.

## Supplementary material

The Supplementary Material for this article can be found online at: <https://www.frontiersin.org/articles/10.3389/fnagi.2026.1730480/full#supplementary-material>

- Bell, R. D. (2007). Transport pathways for clearance of human Alzheimer's amyloid beta-peptide and apolipoproteins E and J in the mouse central nervous system. *J. Cereb. Blood Flow Metab.* 27, 909–918. doi: 10.1038/sj.jcbfm.9600419
- Bellenguez, C., Küçükali, F., Jansen, I. E., Klei, E. D., Moreno-Grau, S., Amin, N., et al. (2022). New insights into the genetic etiology of Alzheimer's disease and related dementias. *Nat. Genet.* 54, 412–436. doi: 10.1038/s41588-022-01024-z
- Bloomfield, P., Bakshi, S., Maass, C., van Maanen, E., Pichardo-Almaraz, C., Yadav, D. B., et al. (2021). Minimal brain PBPK model to support the preclinical and clinical development of antibody therapeutics for CNS diseases. *J. Pharmacokinet. Pharmacodyn.* 48, 861–871. doi: 10.1007/s10928-021-09776-7
- Bloomfield, P., Bumbaca-Yadav, D., Sugam, J., Grauer, S., Smith, B., Antonenko, S., et al. (2022). PBPK-PD modeling for the preclinical development and clinical translation of tau antibodies for Alzheimer's disease. *Front. Pharmacol.* 13:867457. doi: 10.3389/fphar.2022.867457
- Brothers, H. M., Gosztyla, M. L., and Robinson, S. R. (2018). The physiological roles of amyloid- $\beta$  peptide hint at new ways to treat Alzheimer's disease. *Front. Aging Neurosci.* 10:118. doi: 10.3389/fnagi.2018.00118
- Chai, A. B., Lam, H. H. J., Kockx, M., and Gelissen, I. C. (2021). Apolipoprotein E isoform-dependent effects on the processing of Alzheimer's amyloid- $\beta$ . *Biochim. Biophys. Acta BBA-Mol. Cell Biol. Lipids* 1866:158980. doi: 10.1016/j.bbalip.2021.158980
- Chai, A. B., Leung, G. K., Callaghan, R., and Gelissen, I. C. (2020). P-glycoprotein: a role in the export of amyloid- $\beta$  in Alzheimer's disease? *FEBS J.* 287, 612–625. doi: 10.1111/febs.15148
- Chamberland, É., Moravveji, S., Doyon, N., and Duchesne, S. (2024). A computational model of Alzheimer's disease at the nano, micro, and macroscales. *Front. Neuroinformatics* 18:1348113. doi: 10.3389/fninf.2024.1348113
- Chiu, C., Miller, M. C., Monahan, R., Osgood, D. P., Stopa, E. G., and Silverberg, G. D. (2015). P-glycoprotein expression and amyloid accumulation in human aging and Alzheimer's disease: preliminary observations. *Neurobiol. Aging* 36, 2475–2482. doi: 10.1016/j.neurobiolaging.2015.05.020
- Chow, V. W., Mattson, M. P., Wong, P. C., and Gleichmann, M. (2010). An overview of APP processing enzymes and products. *Neuromolecular Med.* 12, 1–12. doi: 10.1007/s12017-009-8104-z
- Chu, J., Zhang, W., Liu, Y., Gong, B., Ji, W., Yin, T., et al. (2024). Biomaterials-based anti-inflammatory treatment strategies for Alzheimer's disease. *Neural Regen. Res.* 19, 100–115. doi: 10.4103/1673-5374.374137
- Clauszitzer, D., Pichardo-Almaraz, C., Relo, A. L., van Bergeijk, J., van der Kam, E., Laplanche, L., et al. (2018). Quantitative systems pharmacology model for Alzheimer disease indicates targeting sphingolipid dysregulation as potential treatment option. *CPT Pharmacometrics Syst. Pharmacol.* 7, 759–770. doi: 10.1002/psp4.12351
- Deane, R., Sagare, A., Hamm, K., Parisi, M., Lane, S., Finn, M. B., et al. (2008). apoE isoform-specific disruption of amyloid  $\beta$  peptide clearance from mouse brain. *J. Clin. Invest.* 118, 4002–4013. doi: 10.1172/JCI36663
- Doshi, V., Joshi, G., Sharma, S., and Choudhary, D. (2024). Gene therapy: an alternative to treat Alzheimer's disease. *Naunyn-Schmiedeberg's Arch. Pharmacol.* 397, 3675–3693. doi: 10.1007/s00210-023-02873-z
- Erdo, F., and Krajcsi, P. (2019). Age-related functional and expression changes in efflux pathways at the blood-brain barrier. *Front. Aging Neurosci.* 11:196. doi: 10.3389/fnagi.2019.00196
- Fan, D.-Y., and Wang, Y.-J. (2020). Early intervention in Alzheimer's disease: how early is early enough? *Neurosci. Bull.* 36, 195–197. doi: 10.1007/s12264-019-00429-x
- Ferl, G. Z., Fuji, R. N., Atwal, J. K., Sun, T., Ramanujan, S., and Quartino, A. L. (2020). Mechanistic modeling of soluble A $\beta$  dynamics and target engagement in the brain by anti-A $\beta$  mAbs in Alzheimer's disease. *Curr. Alzheimer Res.* 17, 393–406. doi: 10.2174/1567205017666200302122307
- Fernández-Calle, R., Konings, S. C., Frontiñán-Rubio, J., García-Revilla, J., Camprubí-Ferrer, L., Svensson, M., et al. (2022). APOE in the bullseye of neurodegenerative diseases: impact of the APOE genotype in Alzheimer's disease pathology and brain diseases. *Mol. Neurodegener.* 17, 62. doi: 10.1186/s13024-022-00566-4
- Fišar, Z. (2022). Linking the amyloid, tau, and mitochondrial hypotheses of Alzheimer's disease and identifying promising drug targets. *Biomolecules* 12:1676. doi: 10.3390/biom12111676
- Foster-Powell, A., Rostami-Hodjegan, A., Meno-Tetang, G., Mager, D. E., and Ogungbenro, K. (2025). Mathematical modeling of neuroinflammation in neurodegenerative diseases. *CPT Pharmacometrics Syst. Pharmacol.* 14, 1908–1922. doi: 10.1002/psp4.70064
- Fu, J., Lai, X., Huang, Y., Bao, T., Yang, J., Chen, S., et al. (2023). Meta-analysis and systematic review of peripheral platelet-associated biomarkers to explore the pathophysiology of Alzheimer's disease. *BMC Neurol.* 23:66. doi: 10.1186/s12883-023-03099-5
- Gamez, N., and Morales, R. (2025). Role of peripheral amyloid- $\beta$  aggregates in Alzheimer's disease: mechanistic, diagnostic, and therapeutic implications. *Neural Regen. Res.* 20, 1087–1089. doi: 10.4103/NRR.NRR-D-24-00066
- Geerts, H., Bergeler, S., Lytton, W. W., and van der Graaf, P. H. (2024a). Computational neurosciences and quantitative systems pharmacology: a powerful combination for supporting drug development in neurodegenerative diseases. *J. Pharmacokinet. Pharmacodyn.* 51, 563–573. doi: 10.1007/s10928-023-09876-6
- Geerts, H., Bergeler, S., Walker, M., Rose, R. H., and van der Graaf, P. H. (2024b). Quantitative systems pharmacology-based exploration of relevant anti-amyloid therapy challenges in clinical practice. *Alzheimers Dement. Transl. Res. Clin. Interv.* 10:e12474. doi: 10.1002/trc2.12474
- Geerts, H., Bergeler, S., Walker, M., van der Graaf, P. H., and Courade, J.-P. (2023a). Analysis of clinical failure of anti-tau and anti-synuclein antibodies in neurodegeneration using a quantitative systems pharmacology model. *Sci. Rep.* 13:14342. doi: 10.1038/s41598-023-41382-0
- Geerts, H., Walker, M., Rose, R., Bergeler, S., van Der Graaf, P. H., Schuck, E., et al. (2023b). A combined physiologically-based pharmacokinetic and quantitative systems pharmacology model for modeling amyloid aggregation in Alzheimer's disease. *CPT Pharmacometrics Syst. Pharmacol.* 12, 444–461. doi: 10.1002/psp4.12912
- Geerts, H., Wiksw, J., van der Graaf, P. H., Bai, J. P., Gaiteri, C., Bennett, D., et al. (2020). Quantitative systems pharmacology for neuroscience drug discovery and development: current status, opportunities, and challenges. *CPT Pharmacometrics Syst. Pharmacol.* 9, 5–20. doi: 10.1002/psp4.12478
- Granhölm, A.-C., and Hamlett, E. D. (2024). The role of tau pathology in Alzheimer's disease and Down syndrome. *J. Clin. Med.* 13:1338. doi: 10.3390/jcm13051338
- Guo, S., Wang, H., and Yin, Y. (2022). Microglia polarization from M1 to M2 in neurodegenerative diseases. *Front. Aging Neurosci.* 14:815347. doi: 10.3389/fnagi.2022.815347
- Gustavsson, A., Norton, N., Fast, T., Frölich, L., Georges, J., Holzapfel, D., et al. (2023). Global estimates on the number of persons across the Alzheimer's disease continuum. *Alzheimers Dement.* 19, 658–670. doi: 10.1002/alz.12694
- Hampel, H., Caraci, F., Cuello, A. C., Caruso, G., Nisticò, R., Corbo, M., et al. (2020). A path toward precision medicine for neuroinflammatory mechanisms in Alzheimer's disease. *Front. Immunol.* 11:456. doi: 10.3389/fimmu.2020.00456
- Hampel, H., Toschi, N., Babiloni, C., Baldacci, F., Black, K. L., Bokde, A. L., et al. (2018). Revolution of Alzheimer precision neurology. Passageway of systems biology and neurophysiology. *J. Alzheimers Dis.* 64, S47–S105. doi: 10.3233/JAD-179932
- Hasegawa, I., Hirayoshi, Y., Minatani, S., Mino, T., Takeda, A., and Itoh, Y. (2022). In vivo dynamic movement of polymerized amyloid  $\beta$  in the perivascular space of the cerebral cortex in mice. *Int. J. Mol. Sci.* 23:6422. doi: 10.3390/ijms23126422
- Jack Jr, C. R., Wiste, H. J., Lesnick, T. G., Weigand, S. D., Knopman, D. S., Vemuri, P., et al. (2013a). Brain  $\beta$ -amyloid load approaches a plateau. *Neurology* 80, 890–896. doi: 10.1212/WNL.0b013e3182840bbe
- Jack, C. R., Knopman, D. S., Jagust, W. J., Petersen, R. C., Weiner, M. W., Aisen, P. S., et al. (2013b). Tracking pathophysiological processes in Alzheimer's disease: an updated hypothetical model of dynamic biomarkers. *Lancet Neurol.* 12, 207–216. doi: 10.1016/S1474-4422(12)70291-0
- Jones, A., Ali, M. U., Kenny, M., Mayhew, A., Mokashi, V., He, H., et al. (2024). Potentially modifiable risk factors for dementia and mild cognitive impairment: an umbrella review and meta-analysis. *Dement. Geriatr. Cogn. Disord.* 53, 91–106. doi: 10.1159/000536643
- Kanekiyo, T., Liu, C.-C., Shinohara, M., Li, J., and Bu, G. (2012). LRP1 in brain vascular smooth muscle cells mediates local clearance of Alzheimer's amyloid- $\beta$ . *J. Neurosci.* 32, 16458–16465. doi: 10.1523/JNEUROSCI.3987-12.2012
- Kanekiyo, T., Xu, H., and Bu, G. (2014). ApoE and A $\beta$  in Alzheimer's disease: accidental encounters or partners? *Neuron* 81, 740–754. doi: 10.1016/j.neuron.2014.01.045
- Karelina, T., Demin, J., O., Demin, O., Duvvuri, S., and Nicholas, T. (2017). Studying the progression of amyloid pathology and its therapy using translational longitudinal model of accumulation and distribution of amyloid beta. *CPT Pharmacometrics Syst. Pharmacol.* 6, 676–685. doi: 10.1002/psp4.12249
- Karelina, T., Lerner, S., Stepanov, A., Meerson, M., and Demin, O. (2021). Monoclonal antibody therapy efficacy can be boosted by combinations with other treatments: Predictions using an integrated Alzheimer's Disease Platform. *CPT Pharmacometrics Syst. Pharmacol.* 10, 543–550. doi: 10.1002/psp4.12628
- Knopman, D. S., Amieva, H., Petersen, R. C., Chételat, G., Holtzman, D. M., Hyman, B. T., et al. (2021). Alzheimer disease. *Nat. Rev. Dis. Primers* 7:33. doi: 10.1038/s41572-021-00269-y
- Koutarapu, S., Ge, J., Dulewicz, M., Srikrishna, M., Szadzińska, A., Wood, J., et al. (2025). Chemical imaging delineates A $\beta$  plaque polymorphism across the Alzheimer's disease spectrum. *Nat. Commun.* 16:3889. doi: 10.1038/s41467-025-59085-7
- Kuhn, A. J., Abrams, B. S., Knowlton, S., and Raskatov, J. A. (2020). Alzheimer's disease "non-amyloidogenic" p3 peptide revisited: A case for amyloid- $\alpha$ . *ACS Chem. Neurosci.* 11, 1539–1544. doi: 10.1021/acscchemneuro.0c00160
- Lecy, E. E., Min, H.-K., Apgar, C. J., Maltais, D. D., Lundt, E. S., Albertson, S. M., et al. (2024). Patterns of early neocortical amyloid- $\beta$  accumulation: a PET population-based study. *J. Nucl. Med.* 65, 1122–1128. doi: 10.2967/jnumed.123.267150

- Leng, F., and Edison, P. (2021). Neuroinflammation and microglial activation in Alzheimer disease: where do we go from here? *Nat. Rev. Neurol.* 17, 157–172. doi: 10.1038/s41582-020-00435-y
- Li, X., Yang, Z., Chen, Y., Zhang, S., Wei, G., and Zhang, L. (2023). Dissecting the molecular mechanisms of the co-aggregation of A $\beta$ 40 and A $\beta$ 42 peptides: A REMD simulation study. *J. Phys. Chem. B* 127, 4050–4060. doi: 10.1021/acs.jpcc.3c01078
- Lin, L., Hua, F., Salinas, C., Young, C., Bussiere, T., Apgar, J. F., et al. (2022). Quantitative systems pharmacology model for Alzheimer's disease to predict the effect of aducanumab on brain amyloid. *CPT Pharmacometrics Syst. Pharmacol.* 11, 362–372. doi: 10.1002/psp4.12759
- Loeffler, D. A. (2023). Antibody-mediated clearance of brain amyloid- $\beta$ : mechanisms of action, effects of natural and monoclonal anti-A $\beta$  antibodies, and downstream effects. *J. Alzheimers Dis. Rep.* 7, 873–899. doi: 10.3233/ADR-230025
- Lyoo, C. H., Ikawa, M., Liow, J.-S., Zoghbi, S. S., Morse, C. L., Pike, V. W., et al. (2015). Cerebellum can serve as a pseudo-reference region in Alzheimer disease to detect neuroinflammation measured with PET radioligand binding to translocator protein. *J. Nucl. Med.* 56, 701–706. doi: 10.2967/jnumed.114.146027
- Madras, K., Das, R., Mohmmadabdul, H., Lin, L., Hyman, B. T., Lauffenburger, D. A., et al. (2021). Systematic in silico analysis of clinically tested drugs for reducing amyloid-beta plaque accumulation in Alzheimer's disease. *Alzheimers Dement.* 17, 1487–1498. doi: 10.1002/alz.12312
- Majid, O., Cao, Y., Willis, B. A., Hayato, S., Takenaka, O., Lalovic, B., et al. (2024). Population pharmacokinetics and exposure–response analyses of safety (ARIA-E and isolated ARIA-H) of lecanemab in subjects with early Alzheimer's disease. *CPT Pharmacometrics Syst. Pharmacol.* 13, 2111–2123. doi: 10.1002/psp4.13224
- Marković, M., Milošević, J., Wang, W., and Cao, Y. (2024). Passive immunotherapies targeting amyloid- $\beta$  in Alzheimer's disease: a quantitative systems pharmacology perspective. *Mol. Pharmacol.* 105, 1–13. doi: 10.1124/molpharm.123.000726
- Marr, R. A., and Hafez, D. M. (2014). Amyloid-beta and Alzheimer's disease: the role of neprilysin-2 in amyloid-beta clearance. *Front. Aging Neurosci.* 6:187. doi: 10.3389/fnagi.2014.00187
- Mawuenyega, K. G., Sigurdson, W., Ovod, V., Munsell, L., Kasten, T., Morris, J. C., et al. (2010). Decreased clearance of CNS  $\beta$ -amyloid in Alzheimer's disease. *Science* 330, 1774–1774. doi: 10.1126/science.1197623
- McDade, E., Bednar, M. M., Brashear, H. R., Miller, D. S., Maruff, P., Randolph, C., et al. (2020). The pathway to secondary prevention of Alzheimer's disease. *Alzheimers Dement. Transl. Res. Clin. Interv.* 6:e12069. doi: 10.1002/trc2.12069
- Mendez, M. F. (2017). What is the relationship of traumatic brain injury to dementia? *J. Alzheimers Dis.* 57, 667–681. doi: 10.3233/JAD-161002
- Moravveji, S., Doyon, N., Mashregi, J., and Duchesne, S. (2024). A scoping review of mathematical models covering Alzheimer's disease progression. *Front. Neuroinformatics* 18:1281656. doi: 10.3389/fninf.2024.1281656
- Mroczo, B., Groblewska, M., Litman-Zawadzka, A., Kornhuber, J., and Lewczuk, P. (2018). Amyloid  $\beta$  oligomers (A $\beta$ Os) in Alzheimer's disease. *J. Neural Transm.* 125, 177–191. doi: 10.1007/s00702-017-1820-x
- Nam, Y., Shin, S. J., Kumar, V., Won, J., Kim, S., and Moon, M. (2025). Dual modulation of amyloid beta and tau aggregation and dissociation in Alzheimer's disease: a comprehensive review of the characteristics and therapeutic strategies. *Transl. Neurodegener.* 14:15. doi: 10.1186/s40035-025-00479-4
- Nichols, E., Steinmetz, J. D., Vollset, S. E., Fukutaki, K., Chalek, J., Abd-Allah, F., et al. (2022). Estimation of the global prevalence of dementia in 2019 and forecasted prevalence in 2050: an analysis for the Global Burden of Disease Study 2019. *Lancet Public Health* 7, e105–e125. doi: 10.1002/alz.051496
- Nicolas, J. (2015). Species differences and impact of disease state on BBB. Blood-Brain Barrier Drug Discov. Optim. Brain Expo. CNS Drugs Minimizing Brain Side Eff. Peripher. *Drugs* 66–93. doi: 10.1002/9781118788523.ch4
- Niot, K., Saperia, C., Saif, N., Carlton, C., and Isaacson, R. S. (2024). Alzheimer's disease risk reduction in clinical practice: a priority in the emerging field of preventive neurology. *Nat. Ment. Health* 2, 25–40. doi: 10.1038/s44220-023-00191-0
- Niu, Z., Gui, X., Feng, S., and Reif, B. (2024). Aggregation Mechanisms and Molecular Structures of Amyloid- $\beta$  in Alzheimer's Disease. *Chem. Eur. J.* 30:e202400277. doi: 10.1002/chem.202400277
- Norris, C., Garimella, H. T., Carr, W., Boutté, A. M., Gupta, R. K., and Przekwas, A. J. (2025). Modeling biomarker kinetics of A $\beta$  levels in serum following blast. *Front. Neurol.* 16:1548589. doi: 10.3389/fneur.2025.1548589
- Omura, J. D. (2022). Modifiable risk factors for Alzheimer disease and related dementias among adults aged  $\geq$  45 years—United States, 2019. *MMWR Morb. Mortal. Wkly. Rep.* 71, 680–685. doi: 10.15585/mmwr.mm7120a2
- Oren, O., Taube, R., and Papo, N. (2021). Amyloid  $\beta$  structural polymorphism, associated toxicity and therapeutic strategies. *Cell. Mol. Life Sci.* 78, 7185–7198. doi: 10.1007/s00018-021-03954-z
- Oumata, N., Lu, K., Teng, Y., Cavé, C., Peng, Y., Galons, H., et al. (2022). Molecular mechanisms in Alzheimer's disease and related potential treatments such as structural target convergence of antibodies and simple organic molecules. *Eur. J. Med. Chem.* 240:114578. doi: 10.1016/j.ejmech.2022.114578
- Paul, J. K., Malik, A., Azmal, M., Gulzar, T., Afghan, M. T. R., Talukder, O. F., et al. (2025). Advancing Alzheimer's therapy: computational strategies and treatment innovations. *IBRO Neurosci. Rep.* 18, 270–282. doi: 10.1016/j.ibneur.2025.02.002
- Perosa, V., Oltmer, J., Munting, L. P., Freeze, W. M., Auger, C. A., Scherlek, A. A., et al. (2022). Perivascular space dilation is associated with vascular amyloid- $\beta$  accumulation in the overlying cortex. *Acta Neuropathol.* 143, 331–348. doi: 10.1007/s00401-021-02393-1
- Prince, M., Comas-Herrera, A., Knapp, M., Guerchet, M., and Karagiannidou, M. (2016). *World Alzheimer Report 2016. Improving Healthcare for People Living With Dementia: Coverage, Quality and Costs Now and in the Future*. London: Alzheimer's Disease International.
- Przekwas, A., Friend, T., Teixeira, R., Chen, Z., and Wilkerson, P. (2006). *Spatial Modeling Tools for Cell Biology*. Huntsville, AL: CFD Res Corp.
- Qin, Y., Han, H., Li, Y., Cui, J., Jia, H., Ge, X., et al. (2023). Estimating bidirectional transitions and identifying predictors of mild cognitive impairment. *Neurology* 100, e297–e307. doi: 10.1212/WNL.00000000000021386
- Rafiq, M. S., and Aisen, P. S. (2023). Detection and treatment of Alzheimer's disease in its preclinical stage. *Nat. Aging* 3, 520–531. doi: 10.1038/s43587-023-00410-4
- Ramakrishnan, V., Friedrich, C., Witt, C., Sheehan, R., Pryor, M., Atwal, J. K., et al. (2023). Quantitative systems pharmacology model of the amyloid pathway in Alzheimer's disease: Insights into the therapeutic mechanisms of clinical candidates. *CPT Pharmacometrics Syst. Pharmacol.* 12, 62–73. doi: 10.1002/psp4.12876
- Rey, J., and Sarntinoranont, M. (2018). Pulsatile flow drivers in brain parenchyma and perivascular spaces: a resistance network model study. *Fluids Barriers CNS* 15, 1–11. doi: 10.1186/s12987-018-0105-6
- Rinauro, D. J., Chiti, F., Vendruscolo, M., and Limbocker, R. (2024). Misfolded protein oligomers: Mechanisms of formation, cytotoxic effects, and pharmacological approaches against protein misfolding diseases. *Mol. Neurodegener.* 19:20. doi: 10.1186/s13024-023-00651-2
- Sanz-Blasco, R., Ruiz-Sánchez de León, J. M., Ávila-Villanueva, M., Valentí-Soler, M., Gómez-Ramírez, J., and Fernández-Blázquez, M. A. (2022). Transition from mild cognitive impairment to normal cognition: determining the predictors of reversion with multi-state Markov models. *Alzheimers Dement.* 18, 1177–1185. doi: 10.1002/alz.12448
- Sastre, M., and Gentleman, S. M. (2010). NSAIDs: how they work and their prospects as therapeutics in Alzheimer's disease. *Front. Aging Neurosci.* 2:1555. doi: 10.3389/fnagi.2010.00020
- Scheidt, T., Łapińska, U., Kumita, J. R., Whiten, D. R., and Klenerman, D., Wilson, M. R., et al. (2019). Secondary nucleation and elongation occur at different sites on Alzheimer's amyloid- $\beta$  aggregates. *Sci. Adv.* 5:eaa1112. doi: 10.1126/sciadv.aau3112
- Schipper, H. M. (2011). Apolipoprotein E: implications for AD neurobiology, epidemiology and risk assessment. *Neurobiol. Aging* 32, 778–790. doi: 10.1016/j.neurobiolaging.2009.04.021
- Schreiner, T. G., Schreiner, O. D., Adam, M., and Popescu, B. O. (2023). The Roles of the Amyloid Beta Monomers in Physiological and Pathological Conditions. *Biomedicines* 11:1411. doi: 10.3390/biomedicines11051411
- Seemiller, L. R., Flores-Cuadra, J., Griffith, K. R., Smith, G. C., and Crowley, N. A. (2024). Alcohol and stress exposure across the lifespan are key risk factors for Alzheimer's Disease and cognitive decline. *Neurobiol. Stress* 29:100605. doi: 10.1016/j.jynstr.2024.100605
- Sehar, U., Rawat, P., Reddy, A. P., Kopel, J., and Reddy, P. H. (2022). Amyloid beta in aging and Alzheimer's disease. *Int. J. Mol. Sci.* 23:12924. doi: 10.3390/ijms232112924
- Shi, M., Chu, F., Zhu, F., and Zhu, J. (2024). Peripheral blood amyloid- $\beta$  involved in the pathogenesis of Alzheimer's disease via impacting on peripheral innate immune cells. *J. Neuroinflammation* 21:5. doi: 10.1186/s12974-023-03003-5
- Shibata, M., Yamada, S., Kumar, S. R., Calero, M., Bading, J., Frangione, B., et al. (2000). Clearance of Alzheimer's amyloid- $\beta$  1–40 peptide from brain by LDL receptor-related protein-1 at the blood-brain barrier. *J. Clin. Invest.* 106, 1489–1499. doi: 10.1172/JCI10498
- Shimada, H., Doi, T., Lee, S., and Makizako, H. (2019). Reversible predictors of reversion from mild cognitive impairment to normal cognition: a 4-year longitudinal study. *Alzheimers Res. Ther.* 11, 1–9. doi: 10.1186/s13195-019-0480-5
- Shinohara, M., Tachibana, M., Kanekiyo, T., and Bu, G. (2017). Role of LRP1 in the pathogenesis of Alzheimer's disease: evidence from clinical and preclinical studies: Thematic Review Series: ApoE and Lipid Homeostasis in Alzheimer's Disease. *J. Lipid Res.* 58, 1267–1281. doi: 10.1194/jlr.R075796
- Song, C., Zhang, T., and Zhang, Y. (2022). Conformational essentials responsible for neurotoxicity of A $\beta$ 2 aggregates revealed by antibodies against oligomeric A $\beta$ 2. *Molecules* 27:6751. doi: 10.3390/molecules27196751
- Teunissen, C. E., Chiu, M.-J., Yang, C.-C., Yang, S.-Y., Scheltens, P., Zetterberg, H., et al. (2018). Plasma amyloid- $\beta$  (A $\beta$ 42) correlates with cerebrospinal fluid A $\beta$ 42 in Alzheimer's disease. *J. Alzheimers Dis.* 62, 1857–1863. doi: 10.3233/JAD-170784

- Thomas, J. H. (2019). Fluid dynamics of cerebrospinal fluid flow in perivascular spaces. *J. R. Soc. Interface* 16:20190572. doi: 10.1098/rsif.2019.0572
- Tolar, M., Hey, J., Power, A., and Abushakra, S. (2021). Neurotoxic soluble amyloid oligomers drive Alzheimer's pathogenesis and represent a clinically validated target for slowing disease progression. *Int. J. Mol. Sci.* 22:6355. doi: 10.3390/ijms22126355
- Tolar, M., Hey, J. A., Power, A., and Abushakra, S. (2024). The single toxin origin of Alzheimer's disease and other neurodegenerative disorders enables targeted approach to treatment and prevention. *Int. J. Mol. Sci.* 25:2727. doi: 10.3390/ijms25052727
- Uleman, J. F., Quax, R., Melis, R. J., Hoekstra, A. G., and Rikkert, M. G. O. (2024). The need for systems thinking to advance Alzheimer's disease research. *Psychiatry Res.* 333:115741. doi: 10.1016/j.psychres.2024.115741
- van der Flier, W. M., de Vugt, M. E., Smets, E. M., Blom, M., and Teunissen, C. E. (2023). Towards a future where Alzheimer's disease pathology is stopped before the onset of dementia. *Nat. Aging* 3, 494–505. doi: 10.1038/s43587-023-00404-2
- Vermunt, L., Sikkes, S. A., Van Den Hout, A., Handels, R., Bos, I., Van Der Flier, W. M., et al. (2019). Duration of preclinical, prodromal, and dementia stages of Alzheimer's disease in relation to age, sex, and APOE genotype. *Alzheimers Dement.* 15, 888–898. doi: 10.1016/j.jalz.2019.04.001
- Vom Hofe, I., Stricker, B. H., Ikram, M. K., Wolters, F. J., and Ikram, M. A. (2025). Long-Term Exposure to Non-Steroidal Anti-Inflammatory Medication in Relation to Dementia Risk. *J. Am. Geriatr. Soc.* 73, 1484–1490. doi: 10.1111/jgs.19411
- Wang, D., Chen, F., Han, Z., Yin, Z., Ge, X., and Lei, P. (2021). Relationship Between Amyloid- $\beta$  Deposition and Blood-Brain Barrier Dysfunction in Alzheimer's Disease. *Front. Cell. Neurosci.* 15:695479. doi: 10.3389/fncel.2021.695479
- Wang, J., Fourriere, L., and Gleeson, P. A. (2024). Advances in the cell biology of the trafficking and processing of amyloid precursor protein: impact of familial Alzheimer's disease mutations. *Biochem. J.* 481:1297–1325. doi: 10.1042/BCJ20240056
- Wardlaw, J. M., Benveniste, H., Nedergaard, M., Zlokovic, B. V., Mestre, H., Lee, H., et al. (2020). Perivascular spaces in the brain: anatomy, physiology and pathology. *Nat. Rev. Neurol.* 16, 137–153. doi: 10.1038/s41582-020-0312-z
- Yu, M., Sporns, O., and Saykin, A. J. (2021). The human connectome in Alzheimer disease—relationship to biomarkers and genetics. *Nat. Rev. Neurol.* 17, 545–563. doi: 10.1038/s41582-021-00529-1
- Zhou, L., Nguyen, T. D., Wegiel, J., and Li, Y. (2021). Quantifying perivascular space in Alzheimer's disease by MRI relaxometry. *Alzheimers Dement.* 17:e057721. doi: 10.1002/alz.057721